

Playing with dye molecules at the inner and outer surface of zeolite L

Gion Calzaferri *, Dominik Brühwiler, Silke Megelski, Michel Pfenniger,
Marc Pauchard, Brian Hennessy, Huub Maas, André Devaux, Urs Graf

Department of Chemistry and Biochemistry, University of Bern, Freiestrasse 3, CH-3000 Bern 9, Switzerland

Abstract

Plants are masters of transforming sunlight into chemical energy. In the ingenious antenna system of the leaf, the energy of the sunlight is transported by chlorophyll molecules for the purpose of energy transformation. We have succeeded in reproducing a similar light transport in an artificial system on a nano scale. In this artificial system, zeolite L cylinders adopt the antenna function. The light transport is made possible by specifically organized dye molecules, which mimic the natural function of chlorophyll. Zeolites are crystalline materials with different cavity structures. Some of them occur in nature as a component of the soil. We are using zeolite L crystals of cylindrical morphology which consist of a continuous one-dimensional tube system and we have succeeded in filling each individual tube with chains of joined but noninteracting dye molecules. Light shining on the cylinder is first absorbed and the energy is then transported by the dye molecules inside the tubes to the cylinder ends. We expect that our system can contribute to a better understanding of the important light harvesting process which plants use for the photochemical transformation and storage of solar energy. We have synthesized nanocrystalline zeolite L cylinders ranging in length from 300 to 3000 nm. A cylinder of 800 nm diameter, e.g. consists of about 150 000 parallel tubes. Single red emitting dye molecules (oxonine) were put at each end of the tubes filled with a green emitting dye (pyronine). This arrangement made the experimental proof of efficient light transport possible. Light of appropriate wavelength shining on the cylinder is only absorbed by the pyronine and the energy moves along these molecules until it reaches the oxonine. The oxonine absorbs the energy by a radiationless energy transfer process, but it is not able to send it back to the pyronine. Instead it emits the energy in the form of red light. The artificial light harvesting system makes it possible to realize a device in which different dye molecules inside the tubes are arranged in such a way that the whole visible spectrum can be used by conducting light from blue to green to red without significant loss. Such a material could conceivably be used in a dye laser of extremely small size. The light harvesting nanocrystals are also investigated as probes in near-field microscopy, as materials for new imaging techniques and as luminescent probes in biological systems. The extremely fast energy migration, the pronounced anisotropy, the geometrical constraints and the high concentration of monomers which can be realized, have great potential in leading to new photophysical phenomena. Attempts are being made to use the efficient zeolite-based light harvesting system for the development of a new type of thin-layer solar cell in which the absorption of light and the creation of an electron-hole pair are spatially separated as in the natural antenna system of green plants. Synthesis, characterization and applications of an artificial antenna for light harvesting within a certain volume and transport of the electronic excitation energy to a specific place of molecular dimension has been the target of research in many laboratories in which different approaches have been followed. To our knowledge, the system developed by us is the first artificial antenna which works well enough to deserve this name. Many other highly organized dye–zeolite materials of this type can be prepared by similar methods and are expected to show a wide variety of remarkable properties. The largely improved chemical and photochemical stability of dye molecules inserted

* Correspondence and reprints:

E-mail address: gion.calzaferri@iac.unibe.ch (G. Calzaferri).

in an appropriate zeolite framework allows us to work with dyes which otherwise would be considered uninteresting because of their lack of stability. We have developed two methods for preparing well-defined dye–zeolite materials, one of them working at the solid–liquid and the other at the solid–gas interface. Different approaches for preparing similar materials are in situ synthesis (ship in a bottle) or different types of crystallization inclusion synthesis. © 2000 Éditions scientifiques et médicales Elsevier SAS. All rights reserved.

Keywords: Artificial antenna; Energy migration; Energy transfer; Zeolite L; Spectral overlap; Light harvesting

1. Introduction [1]

Zeolite nanocrystals can act as hosts for supramolecular organization of molecules, complexes and clusters, thus encouraging the design of precise functionalities [2,3]. The main role of the zeolite framework is to provide the desired geometry for arranging and stabilizing the incorporated species [4,5]. Focusing on supramolecularly organized dye

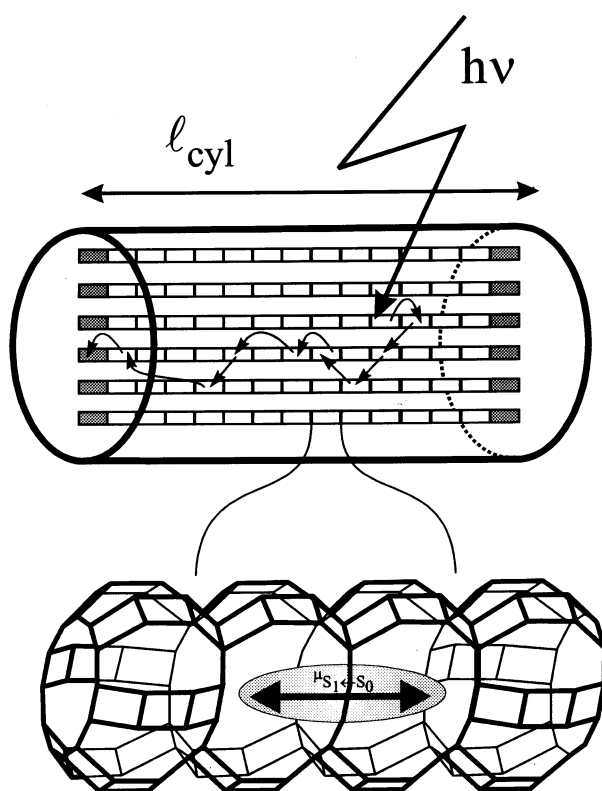


Fig. 1.1. Representation of a cylindrical nanocrystal consisting of organized dye molecules acting as donors (empty rectangles) and an acceptor acting as trap at the front and the back of each channel (shaded rectangles). The enlargement shows a detail of the zeolite L channel with a dye molecule and its electronic transition moment, the ordering of which with respect to the channel axis depends on the length and the shape of the molecule.

molecules in the channels of hexagonal zeolite L crystals we have shown that they provide fascinating possibilities for building an artificial antenna device which consists of highly concentrated monomeric dye molecules in a specific geometrical arrangement [6]. Organic dyes have the tendency to form aggregates even at low concentration [7]. Such aggregates are known to cause fast thermal relaxation of electronic excitation energy. The role of the zeolite is to prevent this aggregation and to superimpose a specific organization. Dye molecules of appropriate size are arranged with their long molecular axis along the one-dimensional channels and they cannot glide past each other because the channels are too narrow. This allows the filling of specific parts of the nanocrystals with a desired type of dye. In such an antenna, light is absorbed by one of the strongly luminescent chromophores. Due to short distances and the ordering of the electronic transition dipole moments of the dyes, the excitation energy is transported by Förster type energy migration [8] preferentially along the axis of the cylindrical antenna to a specific trap. We have recently demonstrated that the insertion of pyronine and oxonine molecules into the channels of zeolite L can be visualized with the help of a fluorescence microscope [9]. One can observe the ordering of the dyes in the channels by means of a polarizer.

Theoretical considerations of energy migration as a series of Förster energy transfer steps have shown that in materials of this kind energy migration rate constants of up to 30 steps/ps or even more can be expected [6]. The principle of the investigated system is illustrated in Fig. 1.1, where the empty bars represent donor molecules, e.g. pyronine, located in the channels of zeolite L. The shaded bars are acceptor molecules, e.g. oxonine, which act as luminescent traps at both ends of the cylinder. We define the occupation probability p as the ratio between the number of sites occupied by a dye molecule and the total number of sites available. A site corresponds to a rectangle. Hence, p adopts values between 0 for an

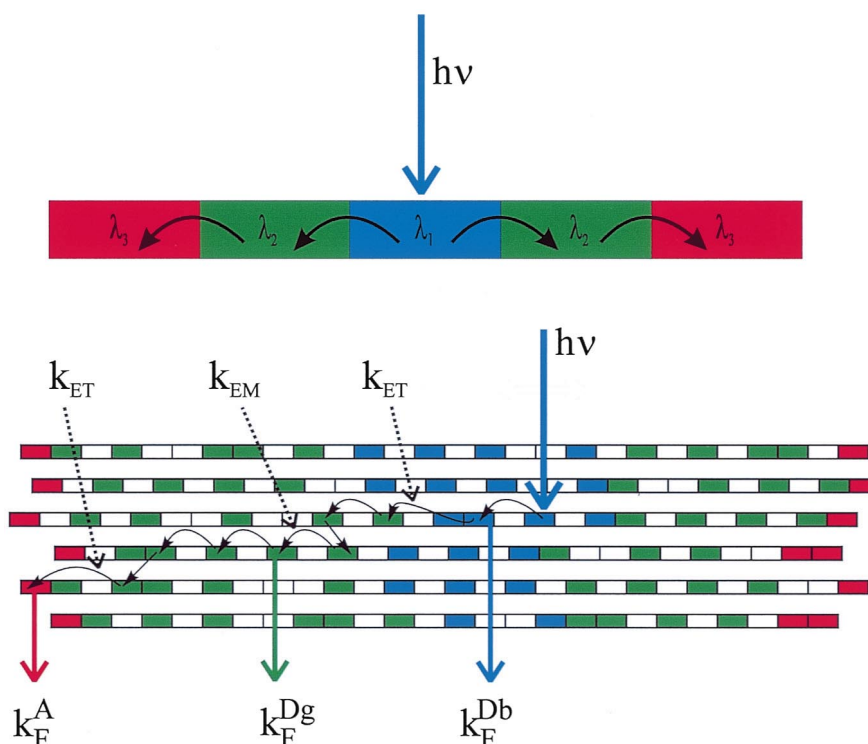


Fig. 1.2. Representation of a bidirectional antenna; $\lambda_1 < \lambda_2 < \lambda_3$. A cylindrical zeolite L nanocrystal containing blue emitting dye molecules in the middle part, followed on both sides by green and then red emitting ones. All dyes are present as monomers and the spectral overlap integrals between the absorption and the emission spectra are sufficiently large. The arrows indicate the direction of energy migration. In the scheme below, only one of the two possible directions is indicated. Both directions are possible in each color region. Once a blue photon has passed into a green or a red region, however, there is no way back. k_{EM} is the rate constant for energy migration, k_{ET} is the rate constant for energy transfer, while k_F^A , k_F^{Dg} and k_F^{Db} are the rate constants for fluorescence of the acceptor and the green (g) and the blue (b) emitting donors. The donor molecules are marked as green and blue rectangles while the acceptors are red [3,12].

unloaded zeolite and 1 for a zeolite loaded to its maximum. The enlargement shows the structure of a zeolite L channel with a donor molecule, the $S_0 \leftrightarrow S_1$ electronic transition moment of which is aligned along the channel axis. A nanocrystal of 600 nm length and a diameter of 800 nm gives rise to more than 150 000 parallel-lying channels, each of which bears a maximum of 400 sites for molecules like oxonine and pyronine.

In the experiments reported in Ref. [10], light is absorbed by a pyronine molecule located somewhere in one of the channels. The excitation energy then migrates along the axis of the nanocrystal, as indicated by the arrows in Fig. 1.1, and is eventually trapped by an oxonine located at the front or at the back of the cylinder. The electronically excited oxonine then emits the excitation energy with a quan-

tum yield of approximately one. We call this process front–back trapping [6].

For some applications it is desirable or even necessary to arrange the nanocrystals as monolayers on a substrate such as a semiconductor, a conducting glass or a metal. An example is a potential new type of a dye-sensitized solar cell. In such a device all incoming light is absorbed within the volume of the nanocrystals of less than 1 μm length containing appropriate dye molecules for light harvesting. The excitation energy is then transported via very fast energy migration to the contact surface with the semiconductor. By efficient (radiationless) energy transfer from an excited dye to the semiconductor, it creates an electron hole pair in the semiconductor. This means that the absorption of light and the creation of an electron hole pair are spatially sepa-

rated, similar to the natural antenna system of green plants. The semiconductor could, for example, consist of a very thin silicon layer which by itself would be much too thin to absorb a significant amount of light. The electron hole pair can then be separated as in an ordinary silicon-based solar cell. This would result in a thin-layer solar cell of only a few μm thickness [2]. We have shown that crystal-monolayers, of the type needed for realizing such a device, can be formed with zeolite A and we are confident that the same will be possible with zeolite L and other zeolite nanocrystals bearing the appropriate morphology (see e.g. figure 4 in Ref. [11]). For such a device monodirectional antenna nanocrystals are needed, while in plastic solar cells and devices based on nano- or microporous materials bidirectional antennae can be used [3]. We have recently been able to prepare a bidirectional antenna with three different dyes, as illustrated in Fig. 1.2 [12].

2. Zeolite L as a host for thin and long stretched dye molecules

Like other hexagonal zeolites, zeolite L consists of linear channels running through the whole nanocrystal (Fig. 2.1). The main channels of zeolite L are made by the stacking of sections with a length of 0.75 nm in the c -direction. The sections are joined by shared 12-membered ring windows having a free diameter of 0.71–0.78 nm. These rings make up the narrowest parts of the main channel. The largest free diameter is about 1.3 nm and lies midway between the 12-membered rings mentioned above [5].

These structural properties determine the kind of material which can be prepared by inserting organic dye molecules into the voids of zeolite L. Only molecules with a diameter less than about 0.75 nm can enter the channels. Molecules of only 1.3 nm length or less can, in principle, be arranged in any direction while longer molecules must align along the c -axis. In addition, the long molecules cannot stack above each other if their kinetic diameter is larger than about 0.4 nm. The anionic framework of zeolite L has another interesting property. Cationic molecules can be inserted by means of cation exchange, while neutral molecules can be inserted from the gas phase, a melt or a solution. The combination

of these two possibilities leads to most interesting materials [12].

Methylviologen MV^{2+} is too short and too flexible to allow reliable predictions concerning its geometrical arrangement in zeolite L. It was therefore worthwhile to consider different possible orientations. On the base of a detailed study including Rietveld refinement of X-ray data and molecular modeling we found that the MV^{2+} lies along the channel wall, and that the angle between the main MV^{2+} axis and the c -axis of the zeolite is 27° [13]. This is illustrated in Fig. 2.2.

MV^{2+} , for which an occupation probability per unit cell of about 0.85 was found, can be considered as a limiting case. Larger and less flexible molecules must align along the c -axis. The occupation probability p is always defined with respect to the number of sites available for a given molecule. This means that p takes values between zero and one, independent of the size of the dye molecules. This definition has many advantages as we will see later.

Zeolite L crystals with cylindrical morphology can be prepared. The c -crystal axis and the long axis of the cylinder coincide [6,14]. An electron microscopy side view of a zeolite L crystal of about 1500 nm is illustrated in Fig. 2.3. In the same Figure we show that in crystals of this size insertion of dyes into the channels can be observed by means of optical fluorescence microscopy. One can see how the molecules penetrate the cylinders from the bottom and the top surface. After an exchange time of 5 min at 98°C with pyronine, its characteristic green fluorescence can be observed at both ends of the cylinder while the section in the middle remains dark. During this short exchange time, the dye molecules coming from both sides only penetrate a small part of the channels. After an exchange time of 2 h, the fluorescent areas have become larger because the dyes on both sides have moved towards the center. If the sample is now exchanged with oxonine for 2 h, a stacking of the molecules inside the tubes is achieved. This is visible by the green emission of the pyronine in the middle and the yellow emission of oxonine near the bottom and the top of the surface. The stacking of the dyes shows that during the oxonine exchange, the inserted pyronine does not leave the zeolite anymore. It also shows that inside the channels the dyes cannot glide past each other.

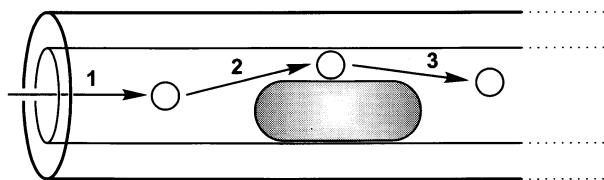


Fig. 2.1. Simplified drawing of a zeolite L channel containing a dye molecule, visualizing the geometrical requirement for a small molecule or ion to pass the dye molecule [19].

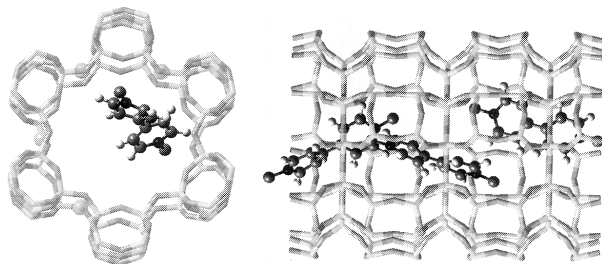


Fig. 2.2. Location of methylviologen in zeolite L. Left: view along the channel axis showing the position and orientation of a molecule. Right: side view of the channel depicting the observed arrangement of the molecules [13].

3. Dyes discussed in this article

The dyes reported in Table 3.1 have been inserted into zeolite L. For additional dyes which have been inserted into zeolite L so far we refer to Refs. [2,12].

Interesting experiments can be made with molecules of similar structure as those inserted into the channels of zeolite L, but which are too large to

enter them and which therefore adsorb only at the outer surface. Out of the many possible examples we give only two in Fig. 3.1 for which some experimental results will be reported.

4. Insertion equilibria

In this chapter we describe equilibria between dyes inside the zeolite L channels and dyes outside either in gas phase or in solution. We assume that the dye molecules only interact with the zeolite framework, including the cations and small molecules like water present in the channels, but that they do not interact with themselves for geometrical reasons. We rely on a recently published study of non interacting particles in microporous materials [15]. Some consequences of results reported there are discussed with respect to the following three cases:

Solid-gas equilibrium: dye molecules D in the gas phase (g) are in equilibrium with dye molecules in the channels of the zeolite Z. The parameter r counts the number of sites occupied by dye molecules. Its values range from 0 to n_{box} . n_{box} is equal to the number of sites in one channel. In case of a 300 nm long zeolite and a 1.5 nm long dye, which occupies two unit cells, n_{box} is equal to 200.



Displacement equilibrium: neutral dye molecules D in the zeolite $\text{ZD}_r\text{X}_{p-x}$ can be displaced by x molecules of X. The states of X(out) and D(out) have to be specified.

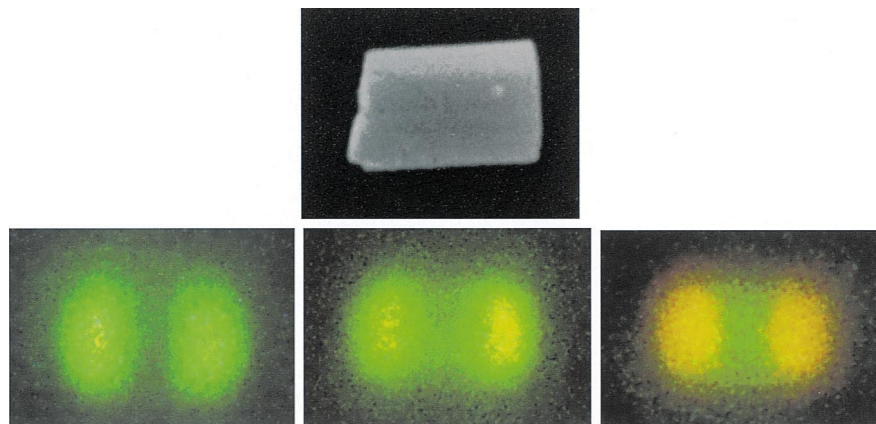
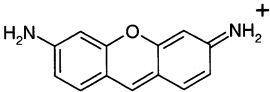
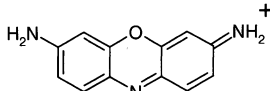
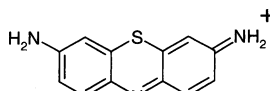
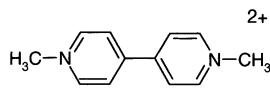
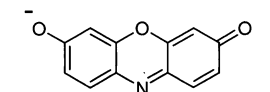
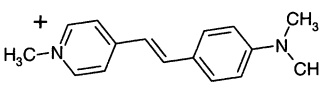
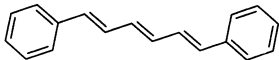
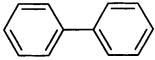


Fig. 2.3. Upper: electron microscopy picture of a zeolite L crystal with a length of 1500 nm. Lower: fluorescence microscope pictures of single zeolite crystals of the same length. Left: after 5 min exchange with pyronine; middle: after 2 h exchange with pyronine; right: after additional 2 h exchange with oxonine [9].

Table 3.1

Names, formulae and approximate values for the maxima of absorption (abs) and emission (em) of inserted dyes discussed in this article

	Ionic dye molecules	abs/em
Pyronine		496 nm/510 nm
Oxonine		582 nm/597 nm
Thionine		620 nm/634 nm
Methyl-viologen		257 nm/ 340 nm (in clay)
Resorufin		560 nm/600 nm
Pyridine dyes		450 nm (protonated 330 nm)/592 nm
	Neutral dye molecules	abs/em
Diphenyl-hexatrien (DPH)		350 nm/425 nm
Biphenyl		247 nm/315 nm
p-Terphenyl		275 nm/339 nm



Ion exchange equilibrium: in most experiments described here, monovalent cationic dyes have been used. D_s^+ and M_s^+ denote the dye cation and the alkali metal cation in solution. Z stands for zeolite and Y describes the cation concentration inside the

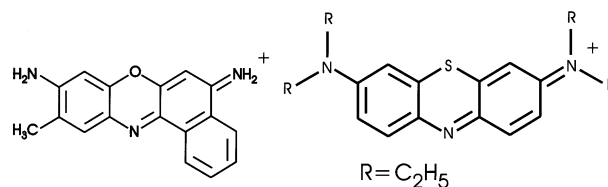


Fig. 3.1. Dyes which only adsorb at the outer surface of zeolite L [16,17]. Left: cresylechtviolett. Right: Ethyleneblue.

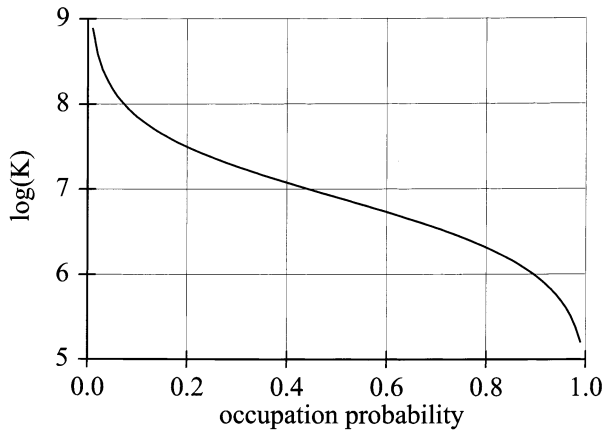
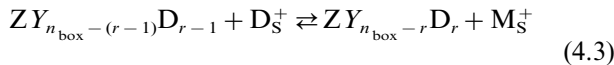


Fig. 4.1. Dependence of the equilibrium constant K for insertion of a dye in zeolite L as a function of the occupation probability p_r , calculated for $K_1 = 7.75 \times 10^8$.

zeolite. For monovalent cations and dyes which occupy two unit cells in zeolite L (e.g. pyronine or oxonine) we must use $Y_{n_{\text{box}}-r} = [(M_{18}^+)_{n_{\text{box}}-r}(M_{17}^+)_r]$ to describe the state of a given channel. An empty site contains 18 M^+ cations. Only one of them can be exchanged by a singly charged dye D^+ cation. By the exchange of rD^+ molecules the number of sites containing 18 cations is reduced by r , and r sites containing only 17 alkali cations are formed.



Using the abbreviation SG for solid–gas, DI for displacement and IE for ion exchange, the equilibrium constants for these three cases can be expressed as follows:

$$K_r^{\text{SG}} = \frac{[ZD_r]}{[ZD_{r-1}][D(\text{g})]} \quad (4.4)$$

$$K_r^{\text{DI}} = \frac{[ZD_r X_{p-x}]}{[ZD_{r-1} X_p][D(\text{out})]^x} \quad (4.5)$$

$$K_r^{\text{IE}} = \frac{[ZY_{n_{\text{box}}-r}D_r]}{[ZY_{n_{\text{box}}-(r-1)}D_{r-1}][D_S^+]} [M_S^+] \quad (4.6)$$

These equations show that the equilibrium constants depend on r . All three cases correspond to the situation expressed in equations (26)–(29) of our study on particle distribution in microporous materials [15]. This means that the r -dependence of the equilibrium constants K_r^{SG} , K_r^{DI} , K_r^{IE} can be described by the same formula:

$$K_{r+1} = K_r \left[\frac{r}{r+1} \frac{n_{\text{box}} - r}{n_{\text{box}} - r + 1} \right] \quad (4.7)$$

It is sufficient to know, e.g. K_1 , from which all other K_r can be calculated. The decrease of K_r with increasing r is due to the fact that the entropy of the system decreases with increasing loading. It is most pronounced for very low or very high loading. This is illustrated in Fig. 4.1 where the dependence of the equilibrium constant K_r as a function of the occupation probability is shown for $K_1 = 7.75 \times 10^8$. From this it follows that the dye insertion is complete for low loading, but that the situation changes for higher loadings. This fact must be taken into account when doing experiments of the type described in this article.

For a better understanding of the consequences of this relation it is useful to discuss an example more explicitly. We choose the ion-exchange equilibrium (4.3). The total concentration of dye molecules inside an ensemble of zeolite nanocrystals dispersed in a solvent $[D_Z]_{\text{tot}}$, expressed with respect to the total volume under consideration, is:

$$[D_Z]_{\text{tot}} = \sum_{r=1}^{n_{\text{box}}} r [ZY_{n_{\text{box}}-r}D_r] \quad (4.8)$$

The total number of channels A_0 , expressed in terms of the total number of zeolite L unit cells uc is given by:

$$A_0 = \frac{uc}{s \cdot n_{\text{box}}} \quad (4.9)$$

where s is the number of unit cells required by one dye molecule ($s=2$ for e.g. pyronine or oxonine).

Using equation (16) of Ref. [15] the individual concentrations $[ZY_{n_{\text{box}}-r}D_r]$ can be expressed as follows:

$$[ZY_{n_{\text{box}}-r}D_r] = \frac{([D_S^+][M_S^+])^r \prod_{j=0}^r K_j}{\sum_{i=0}^{n_{\text{box}}} \left(([D_S^+][M_S^+])^i \prod_{j=0}^i K_j \right)} A_0 \quad (4.10)$$

In this equation $K_0 = 1$, by definition. Using the abbreviation:

$$f_r = \frac{r}{r+1} \frac{n_{\text{box}} - r}{n_{\text{box}} - r + 1} \quad (4.11)$$

and therefore $K_{r+1} = K_r f_r$, and defining $f_0 = 1$, we find after some rearrangement for $r = 1, 2, \dots, n_{\text{box}}$:

$$[ZY_{n_{\text{box}}-r}D_r] = \frac{([D_S^+][M_S^+]K_1)^r \prod_{j=0}^{r-1} f_j^{r-j}}{\sum_{i=0}^{n_{\text{box}}} ([D_S^+][M_S^+]K_1)^i \prod_{j=0}^{i-1} f_j^{i-j}} A_0 \quad (4.12)$$

By using this equation it is possible to calculate the distribution of channels containing a certain amount of dye molecules as a function of the dye concentration in the solvent (see Fig. 4.2).

Eq. (4.12) can be inserted into Eq. (4.8) which leads to the following expression:

$$[D_Z]_{\text{tot}} = \frac{A_0}{1 + \sum_{i=1}^{n_{\text{box}}} \left(([D_S^+][M_S^+]K_1)^i \prod_{j=0}^{i-1} f_j^{i-j} \right) + \sum_{r=1}^{n_{\text{box}}} r ([D_S^+][M_S^+]K_1)^r \prod_{j=0}^{r-1} f_j^{r-j}} \quad (4.13)$$

This equation can be used to determine the equilibrium constant K_1 because the dye concentration in solution $[D_S^+]$, the cation concentration in solution $[M_S^+]$, the total number of channels available A_0 , the number of sites per channel n_{box} , and the total dye concentration $[D_Z]_{\text{tot}}$ can be measured. A numerical solution of Eq. (4.13) is easy to obtain.

Fig. 4.3 shows the total concentration of dye molecules in the channels of zeolite L $[D_Z]_{\text{tot}}$ expressed as occupation probability p , versus the dye concentration in solution in units of the total num-

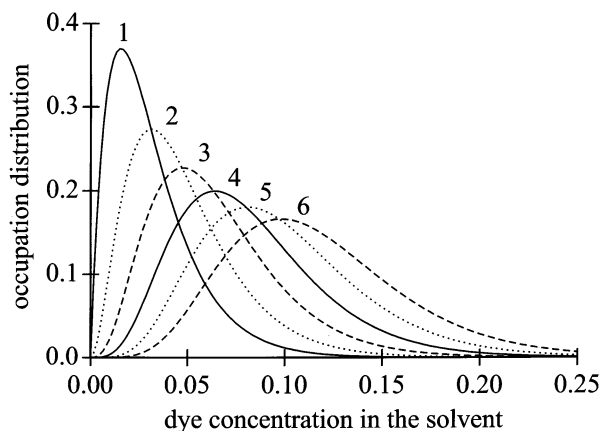


Fig. 4.2. Distribution of channels containing 1, 2, 3, 4, 5 or 6 dye molecules in equilibrium as a function of the dye concentration in the solvent, calculated by means of Eq. (4.12) for: $K_1 = 7.75 \times 10^8$, $[M_S^+] = 1.9 \times 10^{-3}$ M, $n_{\text{box}} = 100$ and $A_0 = 4.4 \times 10^{-7}$ M. The free dye concentration is expressed in units of the total number of available sites $uc/2$.

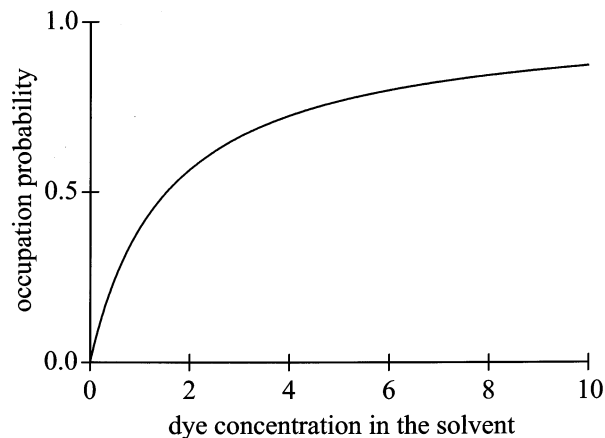


Fig. 4.3. Total concentration $[D_Z]_{\text{tot}}$ of dyes in the channels expressed as occupation probability p , vs. the concentration of free dyes in solution expressed in units of the total number of available sites $uc/2$, calculated with the same parameters as used in Fig. 4.2.

ber of available sites $uc/2$. From the results illustrated it follows that it is easy to prepare materials with low loading but that sophisticated techniques are needed for high loading.

Only few data are available for this kind of analysis. In addition to the pyronine zeolite L data presented above, exchange isotherms have been measured for thionine zeolite L [16] and for methylviologen MV^{2+} . An experimental result for potassium zeolite L suspended in water and exchanged at room temperature is shown in Fig. 4.4. For details see Ref. [13].

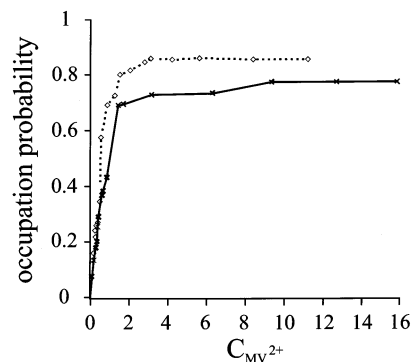


Fig. 4.4. Occupation probability p of the MV^{2+} -loaded zeolite L at room temperature as a function of $C_{MV^{2+}}$, which is the number of mol of MV^{2+} per mol of zeolite L unit cells present in the aqueous suspension. Experiments with self-synthesized zeolite L (dotted) and with commercial zeolite (Linde type ELZ-L, Union Carbide) (solid) [13].

5. Dyes adsorbed at the outer surface

All cationic and neutral dyes have the tendency to adsorb at the outer surface of the zeolite nanocrystals. Their properties at the inner and outer surface of zeolites can be very different. It is therefore useful to make a guess at how many molecules can adsorb as a monolayer on a given amount of zeolite L. The number of molecules n_D needed for a monolayer on a cylinder of equal length and diameter can be expressed as follows:

$$n_D = \frac{A_{zeol}}{A_D} \cdot \frac{1}{N_A} = \frac{m_{zeol}}{\rho_{zeol} l_{cyl}} \cdot \frac{6}{A_D N_A} \quad (5.1)$$

A_{zeol} is the outer surface of the zeolite cylinders, l_{cyl} is their length, ρ_{zeol} is the density, m_{zeol} is the total amount of zeolite in g, A_D is the surface required by one dye lying flat on the zeolite (typically 1.33 nm^2) and N_A is Avogadro's number. For zeolite cylinders of 600 nm average length this leads to:

$$n_D = m_{zeol} \cdot 5.8 \times 10^{-6} \frac{\text{mol}}{\text{g}} \quad (5.2)$$

The number of molecules n_Z which can be placed on one cylinder of equal length and diameter is:

$$n_Z = \frac{3}{2} \pi \frac{l_{cyl}^2}{A_D} \quad (5.3)$$

The number of unit cells uc of a zeolite crystal of radius r_{cyl} is:

$$uc = \frac{2\pi}{\sqrt{3}} l_{cyl} r_{cyl}^2 \frac{1}{|c||a|^2} \quad (5.4)$$

where $|c| = 0.75 \text{ nm}$ and $|a| = 1.85 \text{ nm}$ are the lengths of the unit cell along the corresponding crystal axis.

From this we find that about 10^6 molecules form a monolayer on a 600 nm zeolite L crystal. This number can be compared with the 7.7×10^7 unit cells of such a crystal. It is not yet known under what conditions real monolayers are formed. We expect a large difference in affinity towards the bottom and top surface and the coat. This topic is currently under investigation.

Cationic dye molecules have the tendency to form aggregates on the zeolite surface as can be observed by means of UV-Vis and luminescence spectroscopy. An interesting experiment was reported with thionine [2]: when zeolite L is added to an aqueous thionine solution, aggregates on the zeolite surface are immediately formed, as indicated by the violet color (see Fig. 5.1). When boiling the sample for about 1 min a sudden color change is observed from violet to blue. The dye molecules slip into the zeolite L channels where only monomers can exist for spatial reasons. The blue color remains when the test tube is cooled to room temperature.

In an additional step, not illustrated in Fig. 5.1, we add to the three test tubes on the right a few drops of a 13% hypochlorite solution. The effect is striking: while the color of the first sample on the left fades rapidly, nothing happens to the sample that was boiled. This illustrates how insertion of a dye into an appropriate host can change properties. This experiment is used in our laboratory as a convenient probe to check the success of a zeolite L synthesis. If the test is negative, we can skip the more involved

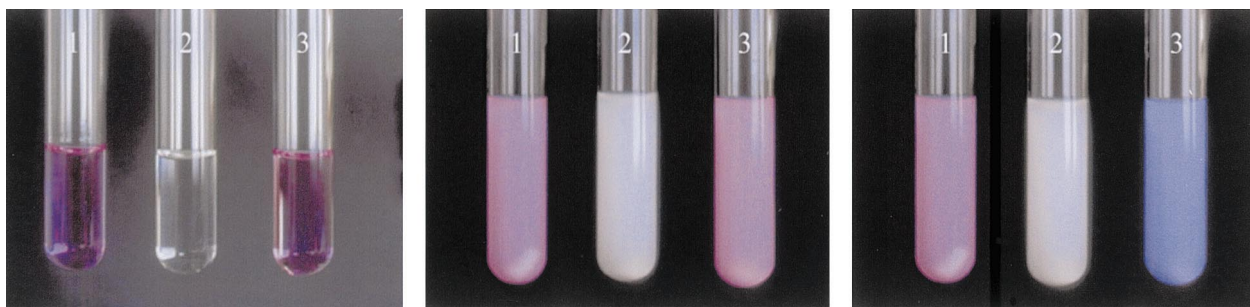


Fig. 5.1. Experiment illustrating the formation of aggregates when zeolite L is added to a solution of thionine in water and the formation of monomers upon heating. Left: two test tubes **1** and **3** containing 4 ml of a $2 \times 10^{-5} \text{ M}$ aqueous solution of thionine monomers. The test tube **2** contains pure water and serves as a reference. Middle: addition of 2 ml of a zeolite suspension (0.2 g zeolite L in 10 ml water) to each of these test tubes results in thionine aggregates immediately formed at the outer surface of the crystals (**1** and **3**). Right: the test tube **3** was heated to near boiling for about 1 min. The color change observed is caused by the molecules entering the channels of the zeolite where they can exist only as monomers.

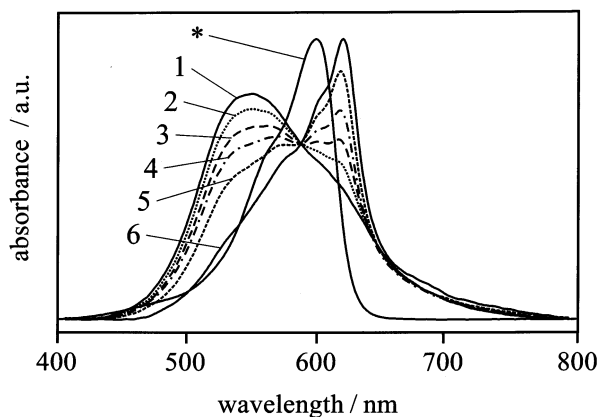
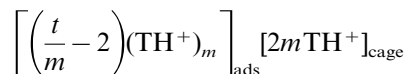
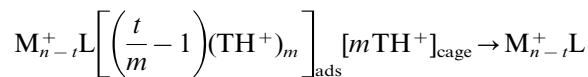
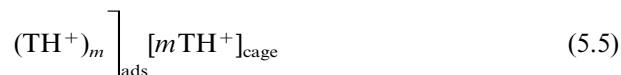
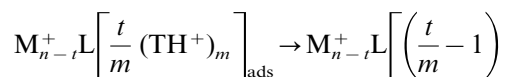


Fig. 5.2. Spectra of a thionine zeolite L suspension in water at 70°C measured at different times after mixing. 1: 0 min; 2: 4 min; 3: 20 min; 4: 2 h; 5: 4 h; 6: 24 h. The spectrum of thionine in aqueous solution (2×10^{-5} M) at room temperature is given as a reference (marked by an asterisk) [16].

powder X-ray and SEM characterization and start a new synthesis. Hypochlorite can also be used to destroy unwanted molecules adsorbed at the outer surface of the zeolite.

More quantitative information is obtained by means of UV–Vis spectroscopy. In Fig. 5.2 we illustrate the change of the absorption spectra of an aqueous dispersion of zeolite L and thionine. These spectra illustrate that the kinetics of the adsorbed dye on the outer zeolite surface $[t/m(\text{TH}^+)_m]_{\text{ads}}$ going into the channels (expressed as $[m\text{TH}^+]_{\text{cage}}$) can be written as follows (for details see Ref. [16]):



m , n and t are stoichiometry coefficients.

The intense band of the aggregates at short wavelengths decreases upon insertion and eventually disappears completely when all of the dye is inserted. It corresponds to what we expect for parallel aggregates [7]. This means that the thionine molecules lie on top of each other in the aggregates, so that their electronic $\pi\pi^*$ transition moments are parallel.

Similar observations have been reported for oxonine [17]. Insertion of this dye can be followed by means of absorption and fluorescence spectroscopy. We observe a band at short wavelengths in the absorption spectrum which disappears with time. The fluorescence intensity increases simultaneously. The aggregates are assumed to be parallel for the same reason as explained for thionine. They quench the fluorescence very efficiently. Oxonine is too large to form aggregates inside the zeolite L channels where its fluorescence is no longer quenched (see Fig. 5.3).

If dye-loaded zeolite L crystals are suspended in a solvent which for steric or polarity reasons cannot enter the zeolite cages, the dyes at the outer surface and those inside the cavities will feel a different environment. Hence they show a different absorption spectrum. The sensitivity of absorption properties towards solvent polarity is called solvatochromy

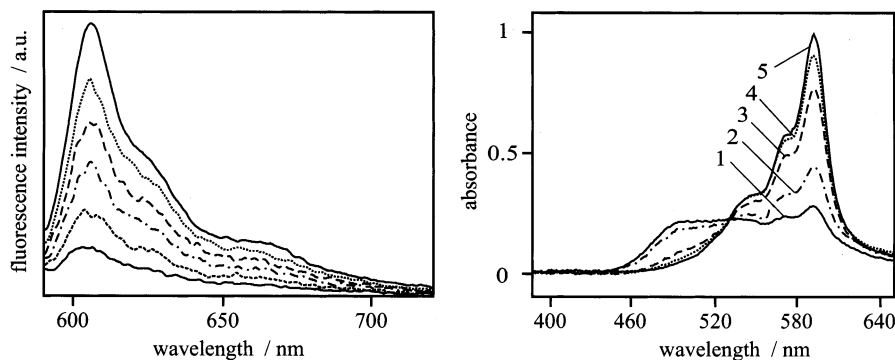


Fig. 5.3. Left: fluorescence spectra of oxonine zeolite L dispersions at r.t. measured at different times after mixing an aqueous zeolite suspension with the dye: 10 s, 30 s, 90 s, 4 min, 4 h, 18 h (bottom to top). The excitation wavelength was 580 nm. Right: absorption spectra measured under the same conditions: 1: 30 s; 2: 9 min; 3: 190 min; 4: 1 day; 5: 7 days [17].

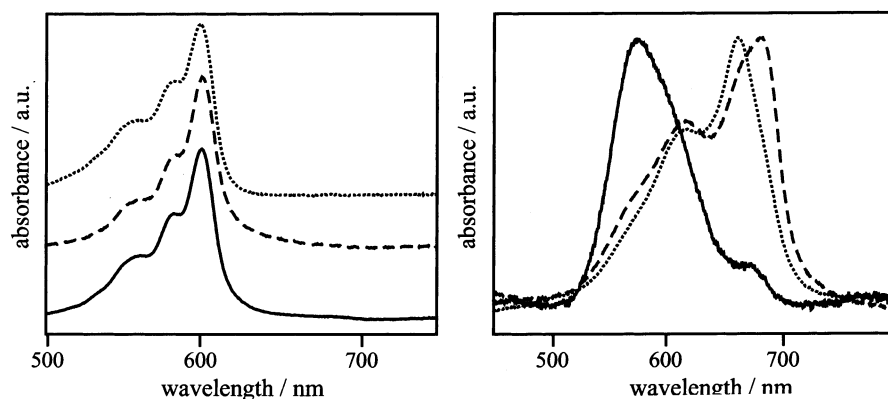


Fig. 5.4. Absorption spectra of oxonine zeolite L (left) and of methyleneblue zeolite L (right) suspensions in different solvents. Cyclohexane (dashed), CH_2BrCl (dotted), water (solid). The spectra on the left are shifted because otherwise they would coincide.

[18]. Fig. 5.4 compares spectra of oxonine which does enter the zeolite L channels and methyleneblue which we found to be too large to enter under the applied conditions [16]. The absorption spectra of the oxonine zeolite L nanocrystals are the same in water, CH_2ClBr and cyclohexane. The spectra of methyleneblue zeolite L samples are, however, significantly different. The dramatic change of the spectrum in water is due to the formation of parallel aggregates.

Additional experiments with molecules located at the outer surface of the zeolite are discussed in Sections 7 and 11.

6. An elegant experiment for visual proof of energy transfer

An experiment for the visual proof of the energy transfer between dyes in zeolite L is based on the observation that pyronine and oxonine cations are incorporated from an aqueous solution with about equal rates. It is therefore possible to realize the situation illustrated in Fig. 6.1 in which the donors are pyronine and the acceptors oxonine molecules. The mean distance between donors D and acceptors A can easily be changed by varying the occupation probability. The main processes in this experiment are energy transfer and luminescence. Energy migration between the donor molecules and between the acceptor molecules, which are of similar probability as the energy transfer, and also radiationless relaxation processes are not indicated.

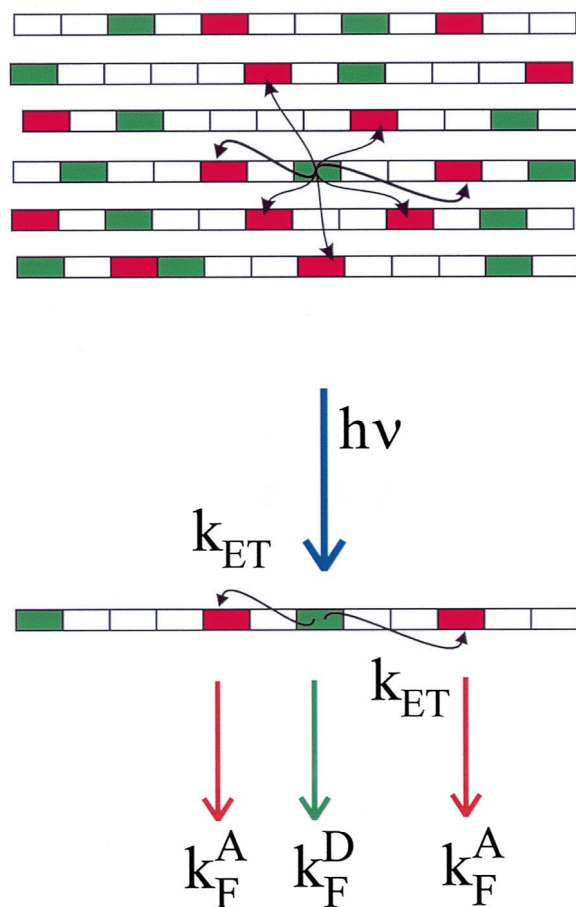


Fig. 6.1. Processes taking place in a zeolite L crystal containing a mixture of donor (pyronine) and acceptor (oxonine) molecules, after excitation of a donor. k_{ET} is the rate constant for energy transfer, while k_{F}^{A} and k_{F}^{D} are the rate constants for fluorescence of the acceptor (red rectangles) and the donor (green rectangles), respectively.

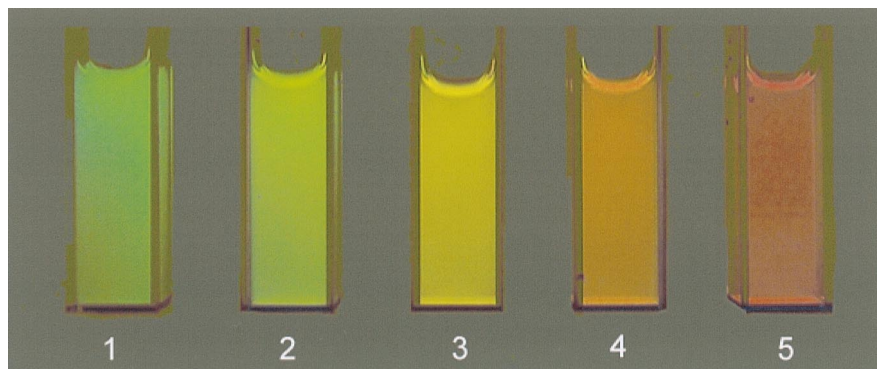


Fig. 6.2. Photographic picture of the fluorescence of suspensions 1–5 after excitation at 256 nm illustrating the increasing pyronine to oxonine energy transfer rate from left to right. The dye concentration inside the nanocrystals is increased in each sample from left to right. The experiment was carried out with zeolite L of 300 nm average length [9].

To carry out the experiment we have two possibilities: the first is to work with a constant total amount of oxonine and pyronine and to vary the amount of zeolite L. The second is to work with a constant amount of zeolite L but to vary the amount of oxonine and pyronine. Both lead to dye-loaded zeolite L nanocrystals with different occupation probabilities and therefore varying donor to acceptor distances. In aqueous dispersions the first type of experiment gives better results for visual demonstration, while the second possibility is more satisfactory for quantitative investigations because light scattering is constant for each sample. The five suspensions illustrated in Fig. 6.2 have been prepared by starting with aqueous solutions containing the same amount of oxonine and pyronine (10^{-6} M). To 2.5 ml of these solutions a decreasing amount of zeolite L (average length of the nanocrystals 300 nm) was added: **1**, 10 mg; **2**, 4 mg; **3**, 2 mg; **4**, 1 mg; **5**, 0.5 mg. Under these conditions incorporation of the dyes is quantitative when boiling the samples under reflux for 2 h. The concentration of each dye inside the nanocrystals was **1**, 5×10^{-4} M; **2**, 1.25×10^{-3} M; **3**, 2.5×10^{-3} M; **4**, 5×10^{-3} M; **5**, 1.0×10^{-2} M. A rough estimate of the mean donor to acceptor distance R_{DA} can be obtained by assuming isotropic conditions:

$$R_{DA} = \left[\frac{3}{4\pi} \cdot \frac{1}{c_A N_A} \right]^{1/3} \quad (6.1)$$

N_A is Avogadro's number and c_A is the concentration of oxonine in the zeolite nanocrystal. From this we obtain the following mean donor–acceptor distances: **1**, 93 Å; **2**, 68 Å; **3**, 54 Å; **4**, 43 Å; **5**, 34 Å.

A more sophisticated theoretical treatment, which takes the anisotropy of the material into account can be found in Ref. [6].

Taking into account radiationless processes, namely internal conversion k_{IC} , intersystem crossing k_{ISC} , and bimolecular quenching $k_Q[Q]$ with a quencher Q, the time-dependent concentrations of the donor D and the acceptor A in the excited singlet state S_1 , $[D_{S_1}]$ and $[A_{S_1}]$ can be expressed as follows:

$$\begin{aligned} \frac{d[D_{S_1}]}{dt} &= j_{abs} - (k_{ET} + k_F^D + k_{IC}^D + k_{ISC}^D + k_Q^D[Q])[D_{S_1}] \\ &= j_{abs} - [D_{S_1}] \sum k_d^D \end{aligned} \quad (6.2)$$

$$\begin{aligned} \frac{d[A_{S_1}]}{dt} &= k_{ET}[D_{S_1}] - (k_F^A + k_{IC}^A + k_{ISC}^A + k_Q^A[Q])[A_{S_1}] \\ &= k_{ET}[D_{S_1}] - [A_{S_1}] \sum k_a^A \end{aligned} \quad (6.3)$$

where j_{abs} is the number of photons absorbed per unit time. The fluorescence quantum yield of the donor Φ_F^D and of the acceptor Φ_F^A under stationary conditions is therefore:

$$\Phi_F^D = \frac{k_F^D}{\sum k_d^D} \quad (6.4)$$

$$\Phi_F^A = \frac{k_{ET} \cdot k_F^A}{\sum k_d^D \sum k_a^A} \quad (6.5)$$

A quantity which in many cases can easily be measured, even in a heterogeneous system, is the ratio between these two fluorescence quantum yields. We therefore write:

$$\frac{\Phi_F^A}{\Phi_F^D} = k_{ET} \cdot \frac{k_F^A}{k_F^D \sum k_a^A} \quad (6.6)$$

This equation shows that the ratio between the acceptor and donor fluorescence quantum yields is directly proportional to the energy transfer rate constant k_{ET} . The rate constant k_{ET}^i for energy transfer from an excited dye molecule on site i to an unexcited one on site j depends on the fluorescence quantum yield Φ_i of the donor in absence of acceptors, on its natural lifetime τ_i , on the refractive index n of the medium, on the geometrical factor G_{ij} , on the spectral overlap J_{ij} of the donor emission and the acceptor absorption spectra, and on the occupation probabilities p_i and p_j of the respective sites [6].

$$k_{ET}^i = \frac{9(\ln 10)}{128\pi^5 N_A n^4} \frac{\Phi_i}{\tau_i} G_{ij} J_{ij} p_i p_j \quad (6.7)$$

The absorption and fluorescence spectra of pyronine and oxonine in Fig. 6.3 illustrate the large pyronine/pyronine, pyronine/oxonine and oxonine/oxonine spectral overlap, which is one of the reasons why these dyes are well suited for these experiments (see Section 8).

The geometrical factor G_{ij} takes into account the influence of the geometrical arrangement of a donor i and an acceptor j . It depends on the distance R_{ij} and on κ_{ij} . The latter describes the relative orientation in space of the transition dipole moments $(\mu_{S_1 \leftarrow S_0})_i$ and $(\mu_{S_1 \leftarrow S_0})_j$ of the donor i and of the acceptor j , respectively:

$$G_{ij} = \frac{\kappa_{ij}^2}{R_{ij}^6} \quad (6.8)$$

For energy transfer from an excited donor \mathbf{d} to acceptors \mathbf{a} , the rate constant k_{ET}^d can be expressed as follows:

$$k_{ET}^d = \sum_a k_{ET}^{da} = \frac{9(\ln 10)}{128\pi^5 N_A n^4} \frac{\Phi_d}{\tau_d} \sum_a G_{da} J_{da} p_a \quad (6.9)$$

In this equation p_d is equal to one and does therefore not appear, because we describe energy transfer from a donor which is excited with a probability equal to one. In addition, we average over many such events taking place in many different nanocrystals with similar geometrical environment $\langle \sum_a G_{da} \rangle$. Since J_{da} also appears as an average quantity, Eq. (6.9) can be

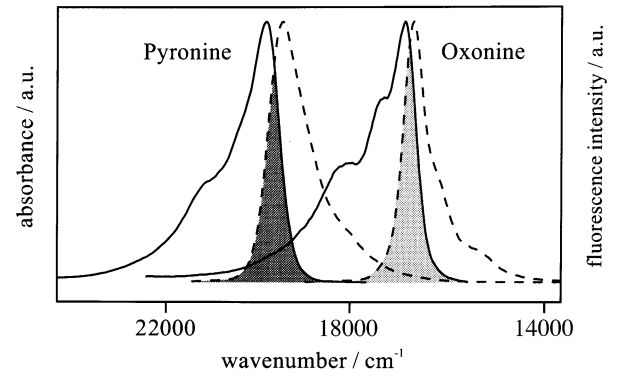


Fig. 6.3. Absorption (solid) and corrected emission (dashed) spectra of pyronine zeolite L and oxonine zeolite L suspended in water. The maxima of all spectra were adjusted to equal height. The spectral overlap regions of the two dyes are shaded; the pyronine/oxonine spectral overlap is not marked.

simplified as follows:

$$k_{ET}^d = \frac{9(\ln 10)}{128\pi^5 N_A n^4} \frac{\Phi_d}{\tau_d} \langle J_{da} \rangle \left\langle \sum_a G_{da} \right\rangle p_a \quad (6.10)$$

Inserting this expression into Eq. (6.6), we obtain [3]:

$$\frac{\Phi_F^A}{\Phi_F^D} = \left\{ \frac{k_F^A}{k_F^D \sum k_a^A} \frac{9(\ln 10)}{128\pi^5 N_A n^4} \frac{\Phi_d}{\tau_d} \langle J_{da} \rangle \left\langle \sum_a G_{da} \right\rangle \right\} p_a \quad (6.11)$$

This equation tells us that the ratio of the acceptor to donor luminescence quantum yield is proportional to the acceptor occupation probability p_a . Provided that all values in the curved brackets are kept constant we can write:

$$\frac{\Phi_F^A}{\Phi_F^D} = C \cdot p_a \quad (6.12)$$

where C is equal to:

$$C = \frac{k_F^A}{k_F^D \sum k_a^A} \frac{9(\ln 10)}{128\pi^5 N_A n^4} \frac{\Phi_d}{\tau_d} \langle J_{da} \rangle \left\langle \sum_a G_{da} \right\rangle \quad (6.13)$$

Eq. (6.12) can best be tested by carrying out the second type of experiment mentioned at the beginning of this chapter, namely by working with a constant amount of zeolite L but by varying the amount of oxonine and pyronine. Under these conditions light scattering is constant. The results of such an experiment are illustrated in Fig. 6.4 for occupations $p_a \approx 2^a \times 0.0015$, $a = 0, 1, \dots, 4$, which cor-

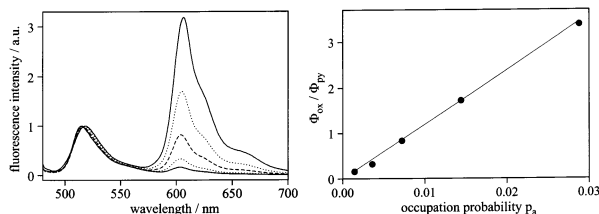


Fig. 6.4. Fluorescence spectroscopic examinations of five suspensions with $p_a = 0.0014, 0.0036, 0.0072, 0.0144$ and 0.0288 after specific excitation of pyronine at 465 nm. Left: fluorescence spectra normalized to the same peak height for the pyronine emission at about 520 nm. The intensity of the oxonine emission (peak on the right) increases with increasing p_a . Right: ratio of the fluorescence intensity Φ_{ox} of the acceptor (oxonine) and the donor (pyronine) Φ_{py} as a function of the loading p_a of the zeolite L.

respond to dye concentrations inside of each nanocrystal of $2^a \times 0.0006$ M. The experiment was carried out with zeolite L of 700 nm average length. The fluorescence spectra on the left side of Fig. 6.4, measured after specific excitation of pyronine, show that at the lowest loading the green emission of pyronine with a maximum at about 520 nm dominates. An increase in the loading causes this emission to decrease and the oxonine emission with a maximum at about 605 nm to increase. At $p = 0.0288$ the oxonine emission clearly dominates. The ratio of the acceptor to donor fluorescence intensity illustrated on the right side of Fig. 6.4 shows that the linear relation (Eq. (6.12)) holds with a constant $C = 121$ site. The bathochromic shift of the maximum of the pyronine emission band is due to self-absorption and re-emission, which will be discussed in Section 9. Data reported in Ref. [9] for experiments

carried out in a slightly different way show the same behavior.

7. Insertion and exit kinetics

The energy transfer in the channels of zeolite L discussed in Section 6 can be used for measuring the insertion kinetics. A situation as illustrated in Fig. 7.1 must be prepared at the beginning of the experiment. Immediately after all dye molecules have entered the zeolite channels maximum energy transfer is observed because the donor to acceptor distance is short. When the molecules diffuse into the channels the donor to acceptor distance increases and hence the energy transfer rate decreases. From this the insertion kinetics can be derived.

From Eqs. (6.6) and (6.7) we find that the ratio of the acceptor to donor fluorescence yield, which is equal to the ratio of the corresponding intensities I , at position z of a microcrystal at time t , is given by:

$$\frac{\Phi_F^A}{\Phi_F^D}(z, t) = \frac{I_F^A}{I_F^D}(z, t) = C \cdot p_A(z, t) \cdot p_D(z, t) \quad (7.1)$$

What we can observe with our instrumentation is an average over the whole microcrystal, which means an average over z :

$$\frac{I_F^A}{I_F^D}(t) = \left\langle \frac{I_F^A}{I_F^D}(z, t) \right\rangle = C \cdot \langle p_A(z, t) \cdot p_D(z, t) \rangle \quad (7.2)$$

where C is given by Eq. (6.13). If an experiment is carried out so that the occupation probabilities $p_A(z, t)$ and $p_D(z, t)$ are equal, they can be expressed as follows:

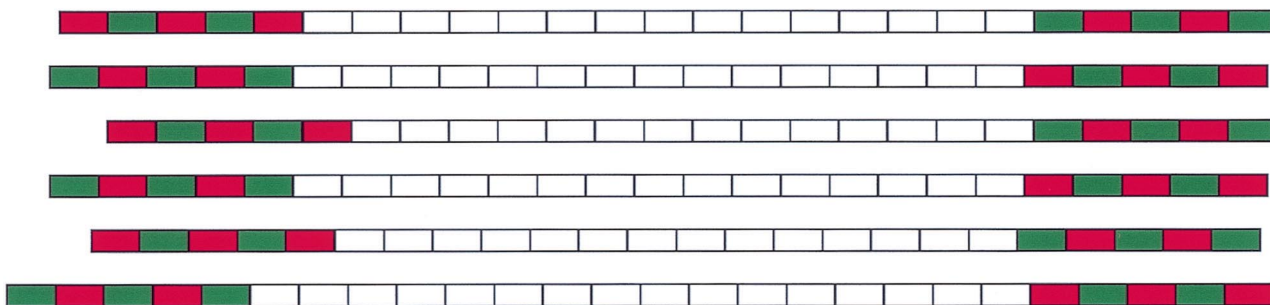


Fig. 7.1. Diffusion of dye molecules in the channels of zeolite L measured by means of Förster energy transfer. An idealized situation at the beginning of the experiment is shown. The donor molecules are marked as green and the acceptors as red rectangles.

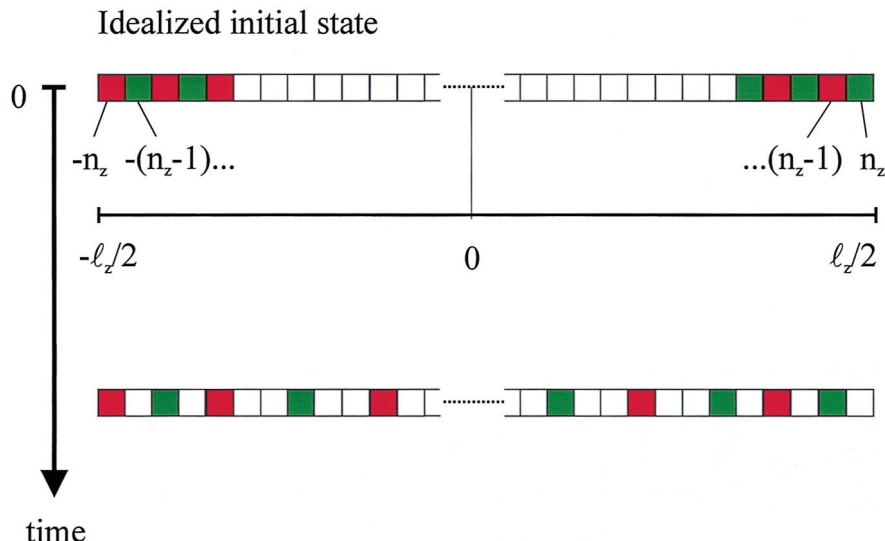


Fig. 7.2. Initial state of a channel and state after diffusion has occurred for some time.

$$p(z, t) = \frac{p^0}{\sqrt{4\pi Dt}} \sum_{-n_z}^{n_z} e^{-(z-n_z)^2/(4Dt)} \quad (7.3)$$

where D is the diffusion coefficient, t the time, p^0 the distribution at time $t = 0$ and $2n_z + 1$ is the number of sites n_{box} in a channel. This situation is illustrated in Fig. 7.2.

If the channels used in an experiment are long enough, so that they consist of at least a few hundred sites, the reasoning can be simplified as follows: first we assume that at time $t = 0$ the system is prepared so that the initial distribution of the donor and the acceptor molecules can be assumed to be equal:

$$p_D^0 \approx p_A^0 \quad (7.4)$$

Then we assume that the number of sites in the channels extends to infinity, so that the situation can be described as illustrated in Fig. 7.3.

Applying these assumptions, the donor and the acceptor distributions can be expressed as follows:

$$p_D(z, t) = \frac{p_D^0}{\sqrt{4\pi Dt}} e^{-z^2/(4Dt)} \quad (7.5)$$

$$p_A(z, t) = \frac{p_A^0}{\sqrt{4\pi Dt}} e^{-z^2/(4Dt)} \quad (7.6)$$

Inserting this into Eq. (7.2) results in:

$$\frac{I_F^A}{I_F^D}(t) = \left\langle \frac{I_F^A}{I_F^D}(z, t) \right\rangle$$

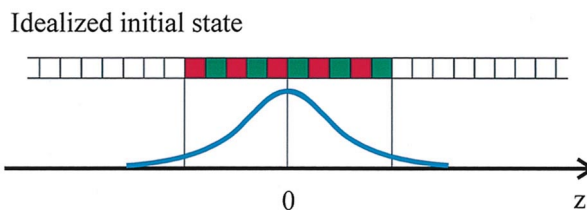


Fig. 7.3. Initial state of a channel extending to infinity. The Gaussian distribution expressed by Eq. (7.5) is also shown.

$$= C \cdot \left\langle \frac{p_A^0}{\sqrt{4\pi Dt}} e^{-z^2/(4Dt)} \cdot \frac{p_D^0}{\sqrt{4\pi Dt}} e^{-z^2/(4Dt)} \right\rangle \quad (7.7)$$

Using Eq. (7.4) this can be expressed as:

$$\frac{I_F^A}{I_F^D}(t) = C \cdot \frac{(p^0)^2}{4\pi Dt} \int_{-\infty}^{\infty} e^{-z^2/(2Dt)} dz \quad (7.8)$$

which leads to:

$$\frac{I_F^A}{I_F^D}(t) = C \cdot \frac{(p^0)^2}{\sqrt{8\pi}} \frac{1}{\sqrt{Dt}} \quad (7.9)$$

The result of an experiment is illustrated in Fig. 7.4. It shows that the $(Dt)^{-1/2}$ dependence is well fulfilled after an initial preparation time.

A different approach was used for measuring the exit kinetics of an anionic dye [19].

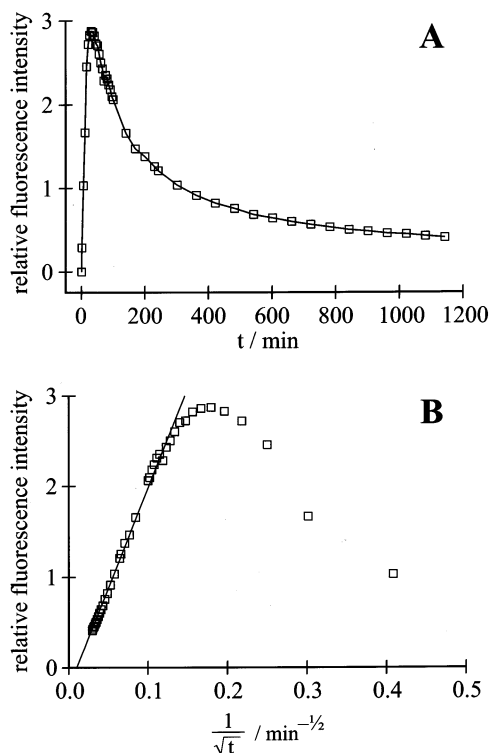


Fig. 7.4. Insertion kinetics observed on zeolite L crystals of 1400 nm length at 80°C in an aqueous suspension. A: relative intensity ($I_F^A/I_P^A(t)$) vs. time. B: relative intensity ($I_F^A/I_P^A(t)$) vs. $1/\sqrt{t}$ and linear regression through the last 20 points on the left.

8. Temperature dependence of the spectral overlap

The spectral overlap J_{ij} is equal to the integral of the corrected and normalized fluorescence intensity $f_i(\bar{\lambda})$ of the donor multiplied by the extinction coefficient $\varepsilon_j(\bar{\lambda})$ of the acceptor as a function of the wave number $\bar{\lambda}$:

$$J_{ij} = \int_0^\infty \varepsilon_j(\bar{\lambda}) f_i(\bar{\lambda}) \frac{d\bar{\lambda}}{\bar{\lambda}^4} \quad (8.1)$$

J_{ij} is expressed in units of $\text{cm}^3 \text{M}^{-1}$.

We have investigated the temperature dependence of the spectral overlap of the following donor/acceptor pairs in the channels of zeolite L: pyronine/pyronine, oxonine/oxonine and pyronine/oxonine. Dye-loaded zeolite L layers were prepared on circular quartz plates (15 mm in diameter) by depositing a calculated volume of an aqueous suspension of dye-loaded zeolite L (occupation $p = 0.01$) and drying overnight. The resulting layers were of about 3000 nm average thickness. Figs. 8.1 and 8.2 show

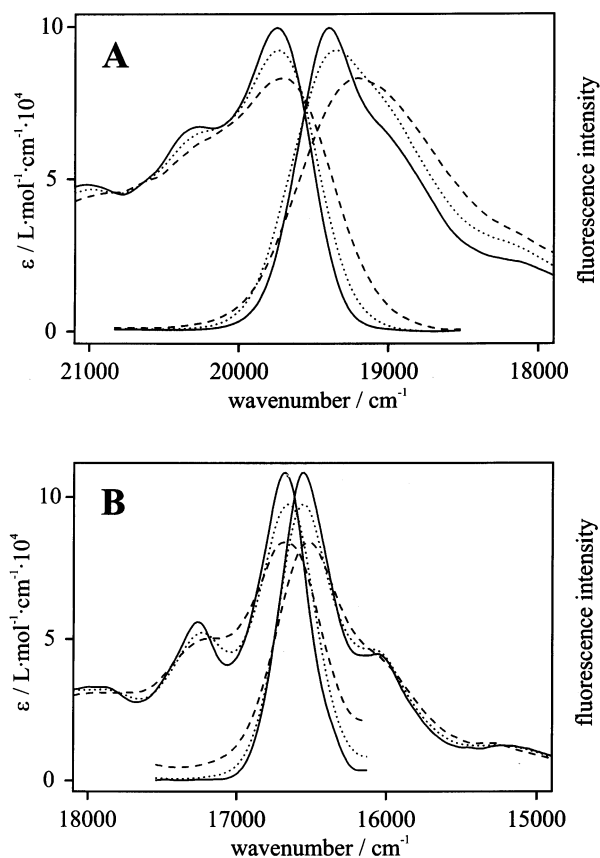


Fig. 8.1. Fluorescence and excitation spectra of pyronine zeolite L (A) and oxonine zeolite L (B) at 80 K (solid), 193 K (dotted) and 293 K (dashed). The fluorescence spectra have been scaled to the same height as the corresponding excitation spectrum.

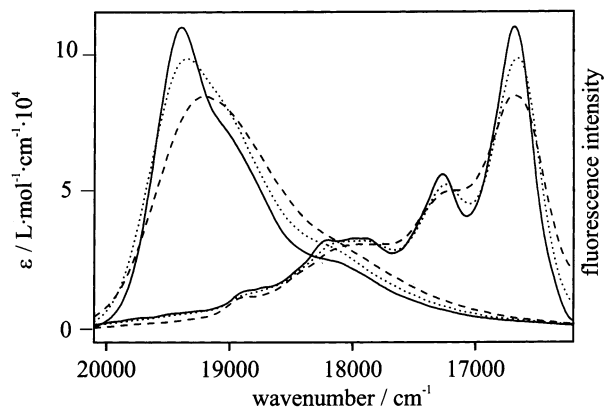


Fig. 8.2. Fluorescence spectra of pyronine zeolite L (left) and excitation spectra of oxonine zeolite L (right) at 80 K (solid), 193 K (dotted) and 293 K (dashed). The fluorescence spectra have been scaled to the same height as the corresponding excitation spectrum.

the excitation and fluorescence spectra for the investigated donor/acceptor pairs at three different temperatures. For a specific dye molecule the maximum of the excitation spectrum measured at room temperature was set equal to the extinction coefficient at the absorption maximum in aqueous solution. The integrals of the excitation spectra were then normalized to the integral of the corresponding spectrum at room temperature. This is reasonable because the oscillator strength f of a transition $n \leftarrow m$ does not depend on the temperature. f can be expressed as follows:

$$f = \frac{8\pi^2 \bar{\lambda} c m_e}{3 h e^2} |\tilde{\mu}_{nm}^{ed}|^2 \quad (8.2)$$

Thereby the electronic transition-dipole moment $\tilde{\mu}_{nm}^{ed}$ between two wave functions ψ_n and ψ_m is defined as:

$$\tilde{\mu}_{nm}^{ed} = \langle \psi_n | \tilde{\mu}_{ed} | \psi_m \rangle \quad (8.3)$$

The oscillator strength is a temperature independent intrinsic property of a molecule. The relation between the molar decadic extinction coefficient ε and the oscillator strength f can be expressed as follows [20]:

$$f = 4.32 \times 10^{-9} \int_{\text{band}} \varepsilon(\bar{\lambda}) d\bar{\lambda} \quad (8.4)$$

The spectral overlap of the investigated donor/acceptor pairs does not change significantly in the temperature range from 80 to 300 K (see Fig. 8.3). The large difference between the absolute values of the overlap integrals of oxonine/oxonine and pyronine/pyronine is due to a different Stokes shift (140 cm^{-1}

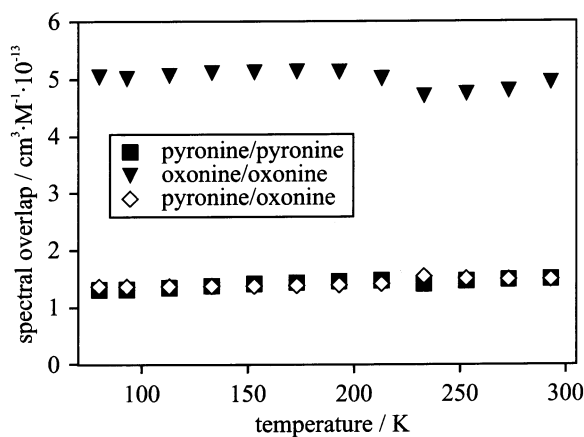


Fig. 8.3. Temperature dependence of the spectral overlap of the investigated donor/acceptor pairs in the channels of zeolite L.

for oxonine, 560 cm^{-1} for pyronine). Note that there is a nice mirror symmetry between excitation and fluorescence spectra for these two cases. This is not given in the case of the pyronine/oxonine overlap integral, which concerns the opposite side of the spectra (low energy side of the fluorescence spectrum and high energy side of the excitation spectrum).

The results shown so far suggest that the spectral overlap between the absorption and fluorescence spectrum of a molecule does not change significantly with temperature. However, there are cases where this is not true. For DPH in zeolite L ($p = 0.5$) we

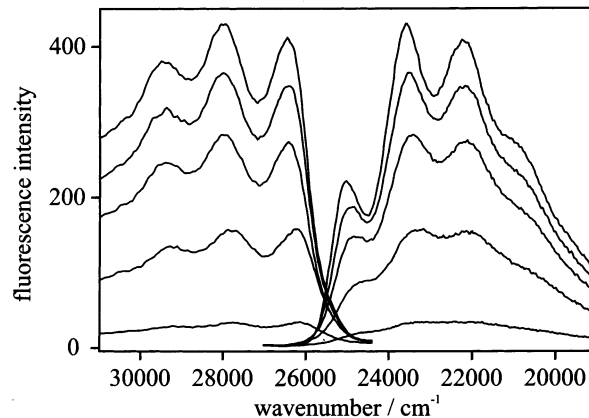


Fig. 8.4. Fluorescence and excitation spectra of DPH-loaded zeolite L at 100, 180, 200, 240 and 293 K (top to bottom). The fluorescence spectra have been scaled to the same height as the corresponding excitation spectrum. The excitation spectra have not been normalized to the same integral in order to demonstrate the decreasing fluorescence intensity with increasing temperatures.

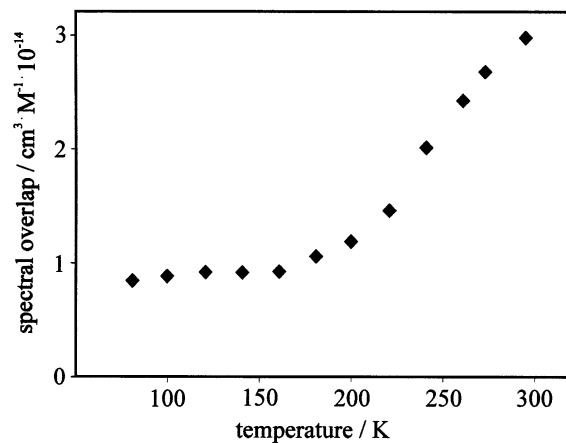
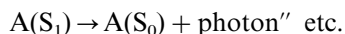
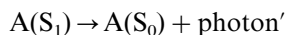


Fig. 8.5. Temperature dependence of the spectral overlap of DPH-loaded zeolite L. Note that the values are ten times smaller compared with the overlap integrals in Fig. 8.3.

found an increasing spectral overlap with increasing temperature. In Fig. 8.4 we chose a different way of presenting the spectra, since the fluorescence quantum yield of DPH strongly depends on the temperature. The excitation spectra were not normalized to the same integral for graphical presentation. Fig. 8.5 compares the values of the spectral overlap integral at different temperatures.

9. Self-absorption and re-emission of fluorescence

A general phenomenon with which we have to be concerned is the fact that there is some overlap between the absorption and the emission spectra for most luminescent organic dyes. This is illustrated in Fig. 6.3 where we show the absorption spectrum of pyronine superimposed on its fluorescence spectrum, as an example. The observed overlap allows a fluorescent photon to be absorbed by a molecule of the same type. Such re-absorption is termed *self-absorption* and the emission of the secondary photons is termed *re-emission*. Depending on the spectral characteristics of a dye, its concentration, its relative orientation, the geometry of the sample and the refractive index of the solvent, several self-absorption and re-emission processes can take place.



Self-absorption and re-emission processes are sometimes called ‘trivial energy transfer mechanisms’ [8]. This term is misleading because the consequences of such processes can be quite complex and interesting [21,22]. We will presently ignore many possible complications and only discuss cases where the line shape of the absorption and of the emission spectra can be thought of as homogeneous due to the rapid exchange that occurs between the various ensembles.

9.1. Spherical geometry

Consequences of self-absorption and re-emission can best be discussed by assuming spherical geometry. This situation is experimentally approached if photons out of a small solid angle are collected, as

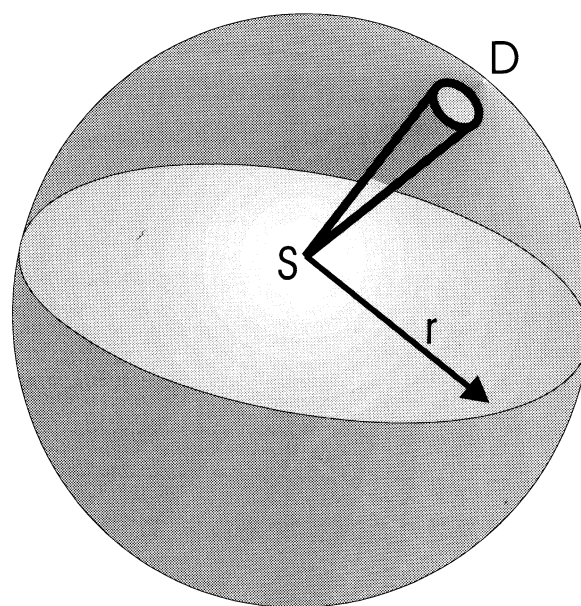


Fig. 9.1. Spherical geometry: S = source of emission and D = point of detection.

illustrated in Fig. 9.1. We further assume that the only concentration-dependent process that can affect the luminescence decay parameters with respect to infinite dilution is self-absorption/re-emission. Our derivation holds for situations where the excitation intensity is low enough so that the concentration of molecules in the excited state is small. The absorption of light by them can therefore be neglected. First, we consider the spectral properties of the re-emitted photons in relation to the emission spectrum at infinite dilution. Second, the time evolution of the first re-emission is calculated for a single exponential decay and also for a sum of single exponential decays.

$E(\lambda)$ describes the normalized emission spectrum at the source of emission and $a(\lambda)$ the absorption probability between the source of emission and the point of detection:

$$a(\lambda) = 1 - 10^{-\varepsilon(\lambda)cr} \quad (9.1)$$

$\varepsilon(\lambda)$ is the molar extinction coefficient, c the concentration in mol/L and r the path length. The total fraction of fluorescence photons a_{tot} absorbed between the source of emission S and the point of detection D in the sample is described by:

$$a_{\text{tot}} = \int_{\lambda} E(\lambda)a(\lambda) d\lambda \quad (9.2)$$

The spectrum of the primary emission $F_0(\lambda)$ at the point of detection is different from $E(\lambda)$, due to self-absorption:

$$F_0(\lambda) = [1 - a(\lambda)]E(\lambda) \quad (9.3)$$

with η as fluorescence quantum yield, we obtain for the first re-emission at the point of detection:

$$F_1(\lambda) = \eta a_{\text{tot}}[1 - a(\lambda)]E(\lambda) = \eta a_{\text{tot}}F_0(\lambda) \quad (9.4)$$

and for the j th re-emission:

$$F_j(\lambda) = (\eta a_{\text{tot}})^j F_0(\lambda) \quad (9.5)$$

The observed total emission $F_T(\lambda)$ is the sum of all contributions:

$$F_T(\lambda) = F_0(\lambda) \sum_{j=0}^n (\eta a_{\text{tot}})^j \quad (9.6)$$

A conclusion which can be drawn is that each emission has the same spectrum $F_0(\lambda)$ if detected at the same point and its shape does not depend on the fluorescence quantum yield. This is correct as long as the emission spectrum $E(\lambda)$ at the source of emission and also the absorption probability $a(\lambda)$ do not change. We illustrate the consequences of self-absorption and re-emission in Fig. 9.2 for pyronine as a typical example for dyes with a large overlap between the absorption and the fluorescence spectrum. For dyes with a smaller spectral overlap the effect is smaller and for dyes with a larger spectral overlap it is even more pronounced.

The example corresponds to a 10^{-5} M concentration in a 1 cm cuvette or a 0.1 M concentration in a

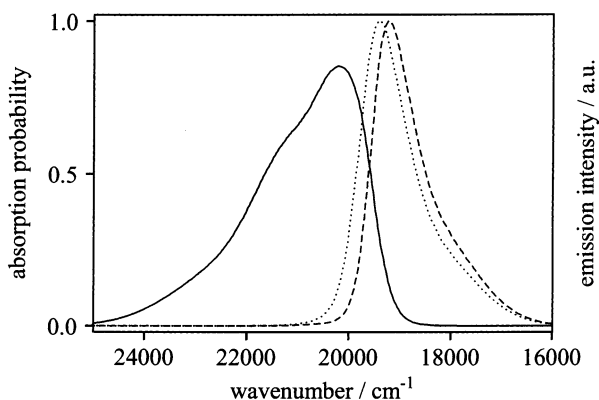


Fig. 9.2. Absorption probability $a(\lambda)$ (solid), emission spectrum at infinite dilution $E(\lambda)$ (dotted) and total emission spectrum $F_T(\lambda)$ (dashed). $E(\lambda)$ and $F_T(\lambda)$ have been scaled to the same height at their respective maxima, while $a(\lambda)$ is shown in absolute values for $rc = 10^{-5}$ M cm, which corresponds to $a_{\text{tot}} = 0.244$.

1000 nm layer with an isotropic transition moment distribution of the molecules. For highly ordered dye molecules and a 1000 nm layer it corresponds to 0.033 M. The calculated shift of the maximum of the fluorescence spectrum $F_T(\lambda)$ as a function of rc for an isotropic distribution is shown in Fig. 9.3. We observe that the shift becomes significant for $rc > 10^{-6}$ M cm and that it increases linearly with $\log(rc)$ above $rc \approx 10^{-5}$ M cm.

Self-absorption and re-emission not only affect the shape of the emission spectrum, but also the fluorescence decay time. We simplify the calculations by assuming that the decay time τ is independent of the emission wavelength and we study a single exponential decay at the source of emission where the fluorescence spectrum is given by $E(\lambda)$. With these simplifications the normalized primary emission $V_0(t)$ after a δ -pulse excitation equals the system's impulse response $T(t)$ at the source of emission and also at some distance, as long as rc is small (typically $rc < 10^{-6}$ M cm).

$$V_0(t) = \frac{1}{\tau} e^{-t/\tau} \quad (9.7)$$

The time evolution of the first re-emission $V_1(t)$ is described by the convolution of the primary emission which acts as excitation source with the impulse response:

$$V_1(t) = \frac{a_{\text{tot}}\eta}{\tau^2} \int_0^t e^{-\theta/\tau} e^{-(t-\theta)/\tau} d\theta \quad (9.8)$$

from which we get:

$$V_1(t) = \frac{a_{\text{tot}}\eta}{\tau} \frac{t}{\tau} e^{-t/\tau} \quad (9.9)$$

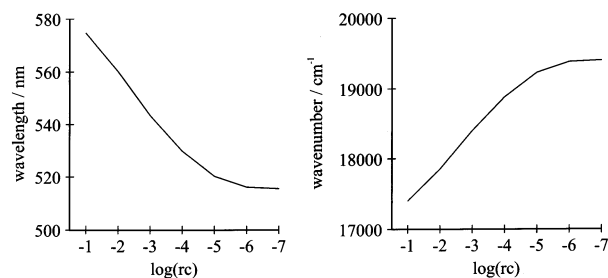


Fig. 9.3. Shift of the fluorescence spectrum due to self-absorption calculated for pyronine as a function of $\log(rc)$; expressed in nm on the left and in cm^{-1} on the right.

$V_1(t)$ is the exciting function of the second re-emission $V_2(t)$. The time evolution of $V_2(t)$ is therefore:

$$V_2(t) = \frac{(a_{\text{tot}}\eta)^2}{\tau^3} \int_0^t \theta e^{-\theta/\tau} e^{-(t-\theta)/\tau} d\theta \quad (9.10)$$

which leads to:

$$V_2(t) = \frac{1}{2} \frac{(a_{\text{tot}}\eta)^2}{\tau} \left(\frac{t}{\tau}\right)^2 e^{-t/\tau} \quad (9.11)$$

$V_3(t)$ and higher terms can be calculated the same way. The time evolution $V_T(t)$ of the fluorescence decay is then given by:

$$V_T(t) = (1 - a_{\text{tot}})[V_0(t) + V_1(t) + V_2(t) + \dots] \quad (9.12)$$

Inserting (9.7), (9.9) and (9.11) we obtain:

$$V_T(t) = (1 - a_{\text{tot}})V_0(t) \left[1 + a_{\text{tot}}\eta \frac{t}{\tau} + \frac{1}{2} \left(a_{\text{tot}}\eta \frac{t}{\tau} \right)^2 + \dots \right] \quad (9.13)$$

The scaling factor $1 - a_{\text{tot}}$ does not influence the decay time and can be omitted. In many practical situations quadratic and higher order terms in $a_{\text{tot}}\eta$ contribute little and can be neglected. We obtain:

$$V_T(t) = \left(1 + a_{\text{tot}}\eta \frac{t}{\tau} \right) \frac{1}{\tau} e^{-t/\tau} \quad (9.14)$$

If the intensity of the excitation source is modulated at a frequency ω we can observe the frequency

response of the emission $T(\omega)$, which is given by the Fourier transform of $V_T(t)$:

$$T(\omega) = \int_0^\infty V_T(t) e^{-i\omega t} dt = \frac{1}{1 + i\omega\tau} + \frac{a_{\text{tot}}\eta}{(1 + i\omega\tau)^2} \quad (9.15)$$

The phase shift $\Phi(\omega)$ between the exciting source and the emitted light is then:

$$\begin{aligned} \tan \Phi(\omega) &= \frac{\text{Im } T(\omega)}{\text{Re } T(\omega)} \\ &= \omega\tau \left(\frac{1 + a_{\text{tot}}\eta - (a_{\text{tot}}\eta)^2}{(1 - \omega^2\tau^2)} \right) \\ &\quad \frac{1}{1 + \omega^2\tau^2 + a_{\text{tot}}\eta(1 - \omega^2\tau^2)} \end{aligned} \quad (9.16)$$

Neglecting higher orders in $a_{\text{tot}}\eta$, this simplifies to:

$$\tan \Phi(\omega) = \omega\tau(1 + a_{\text{tot}}\eta) \quad (9.17)$$

from which we deduce an often used relation between the decay time at infinite dilution $\tau(c \rightarrow 0)$ and the decay time at a concentration c which we name $\tau_{\text{eff}}(c)$:

$$\tau_{\text{eff}}(c) = \tau(c \rightarrow 0)(1 + a_{\text{tot}}\eta) \quad (9.18)$$

The results in Fig. 9.4 indicate that measurements at different concentrations are needed in order to distinguish between cases with and without re-emission, because the shape of the decay curves is well de-

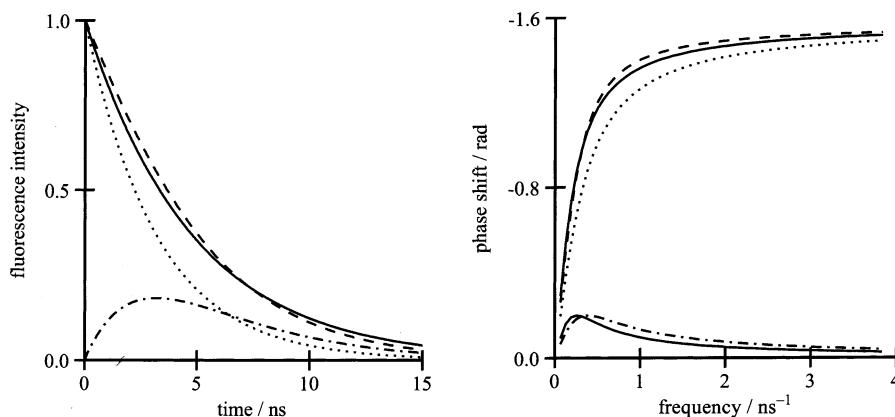


Fig. 9.4. Comparison of a single exponential fluorescence decay with and without self-absorption and re-emission in the time domain (left) and in the frequency domain (right), calculated for $a_{\text{tot}}\eta = 0.5$. Dotted lines illustrate the single exponential decay in the absence of re-emission with $\tau = 3.2$ ns. Solid lines show the behavior of a single exponential decay with an effective decay time $\tau_{\text{eff}} = 4.8$ ns. Dashed lines result in cases of self-absorption and re-emission. The dashdot curve in the time domain graph illustrates the behavior of the re-emission $V_1(t)$. In the frequency domain we show the difference between the phase in presence and in absence of re-emission (dashdot) and the difference between the phase calculated for τ_{eff} and for the exact calculation (solid, lower curve). $V_{\text{eff}}(t)$, $V_0(t)$ and $V_T(t)$ have been scaled to the same height at $t = 0$.

scribed by means of an effective decay time even for large $a_{\text{tot}}\eta$ values, despite of the characteristic form of the re-emission function $V_1(t)$ and despite of the fact that in frequency domain experiments phase differences of less than 1 mrad can be measured. The concentration dependence of the effective decay time τ_{eff} and the extrapolation to infinite dilution Eq. (9.18) was studied in detail for rhodamine 6G [23]. We report data of this study in Table 9.1. They support the conclusion that Eq. (9.18) can be used for values of $a_{\text{tot}}\eta$ up to about 0.1.

Systems can often not be described by a single exponential decay. Multiexponentials or even more complex functions are needed. An extension to multiexponentials is simple. We write:

$$V_0(t) = \frac{1}{\sum_k a_k \tau_k} \sum_k a_k e^{-t/\tau_k} \quad (9.19)$$

The first re-emission is then given by:

$$V_1(t) = a_{\text{tot}}\eta \int_0^t V_0(\theta) V_0(t-\theta) d\theta \quad (9.20)$$

Inserting $V_0(t)$ we obtain:

$$V_1(t) = \frac{a_{\text{tot}}\eta}{\left(\sum_k a_k \tau_k\right)^2} \sum_{k,z} a_k a_z \int_0^t e^{-\theta/\tau_k} e^{-(t-\theta)/\tau_z} d\theta \quad (9.21)$$

which can be expressed as:

$$V_1(t) = \frac{a_{\text{tot}}\eta}{\left(\sum_k a_k \tau_k\right)^2} t \sum_k (a_k)^2 e^{-t/\tau_k} \quad (9.22)$$

$$V_T(t) = \frac{1 - a_{\text{tot}}}{\sum_k a_k \tau_k} \sum_k a_k \left(1 + a_{\text{tot}}\eta \frac{a_k}{\sum_k a_k \tau_k}\right) e^{-t/\tau_k} \quad (9.23)$$

Table 9.1

Rhodamine 6G at different concentrations in ethanol with 5% water^a

Concentration/M	$\tau_{\text{eff}}/\text{ns}$	τ/ns extrapolated $c \rightarrow 0$	a_{tot}
1.03×10^{-5}	4.28	3.87	0.1136
5.15×10^{-6}	4.05	3.83	0.0633
1.03×10^{-6}	3.88	3.83	0.0139
5.15×10^{-7}	3.87	3.84	0.0070
1.03×10^{-7}	3.85	3.85	0.0014

^a Degassed solutions, observed at 540 nm emission wavelength and under magic-angle polarization [23].

Ignoring the scaling factor $(1 - a_{\text{tot}})/\sum_k a_k \tau_k$ and using the abbreviation:

$$b_k = \frac{a_k}{\sum_k a_k \tau_k} \quad (9.24)$$

we can write:

$$V_T(t) = \sum_k a_k (1 + a_{\text{tot}}\eta b_k t) e^{-t/\tau_k} \quad (9.25)$$

If the intensity of the excitation source is modulated at a frequency ω we can observe the frequency response of the emission $T(\omega)$ which is given by the Fourier transform of $V_T(t)$:

$$T(\omega) = \int_0^\infty V_T(t) e^{-i\omega t} dt = \sum_k a_k (1 + a_{\text{tot}}\eta b_k t) \frac{\tau_k}{1 + i\omega\tau_k} + \frac{a_{\text{tot}}\eta}{(1 + i\omega\tau)^2} \quad (9.26)$$

from which we find after some rearrangement:

$$T(\omega) = \sum_k \frac{a_k \tau_k}{1 + (\omega\tau_k)^2} \left(1 + a_{\text{tot}}\eta b_k \tau_k \frac{1 - (\omega\tau_k)^2}{1 + (\omega\tau_k)^2}\right) - i\omega \sum_k \frac{a_k \tau_k^2}{1 + (\omega\tau_k)^2} \left(1 + 2a_{\text{tot}}\eta b_k \tau_k \frac{1}{1 + (\omega\tau_k)^2}\right) \quad (9.27)$$

The phase shift $\Phi(\omega)$ between the exciting source and the emitted light is then:

$$\tan \Phi(\omega) = \frac{\sum_k \frac{a_k \tau_k^2}{1 + (\omega\tau_k)^2} \left(1 + 2a_{\text{tot}}\eta b_k \tau_k \frac{1}{1 + (\omega\tau_k)^2}\right)}{\sum_k \frac{a_k \tau_k}{1 + (\omega\tau_k)^2} \left(1 + a_{\text{tot}}\eta b_k \tau_k \frac{1 - (\omega\tau_k)^2}{1 + (\omega\tau_k)^2}\right)} \quad (9.28)$$

In absence of self-absorption and re-emission a_{tot} is equal to zero. The expressions in the brackets become equal to one and Eq. (9.28) describes the phase shift caused by a multiexponential decay in the absence of self-absorption and re-emission.

We now consider a dual exponential decay with the following components: $\tau_1 = 3.2$ ns, $\tau_2 = 0.2$ ns, $a_2/a_1 = 0.4$ and $a_{\text{tot}} = 0.5$. We observe that it is no longer possible to represent the decay by means of an effective lifetime. The deviations are significant, both in time and in frequency domain measurements (see Fig. 9.5). Experiments carried out at different concentrations are, however, also in such cases useful in order to find a correct interpretation of the system's behavior.

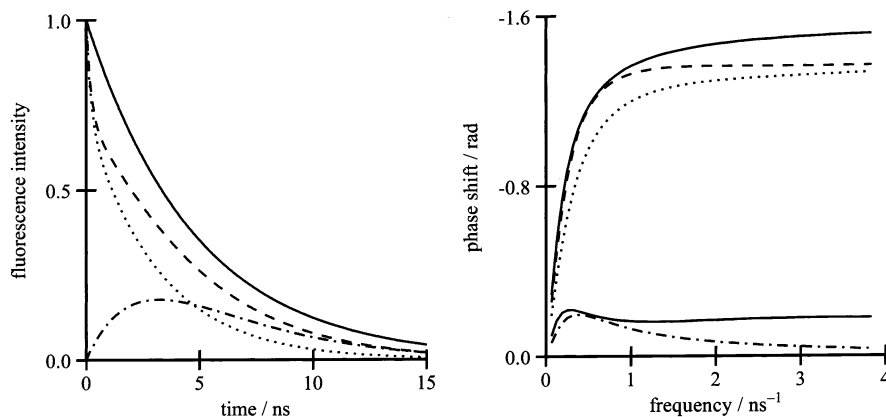


Fig. 9.5. Comparison of a dual exponential fluorescence decay with and without self-absorption and re-emission in the time domain (left) and in the frequency domain (right), calculated for $a_{tot}\eta = 0.5$. Dotted lines illustrate the dual exponential decay in absence of re-emission. The dashed lines result in case of self-absorption and re-emission. Solid lines show the behavior of a single exponential decay with an effective decay time $\tau_{eff} = 4.8$ ns. The dashdot curve in the time domain graph illustrates the behavior of the re-emission $V_1(t)$. In the frequency domain we show the difference between the phase in presence and in absence of re-emission (dashdot) and the difference between the phase calculated for τ_{eff} and for the exact calculation (solid, lower curve). $V_{eff}(t)$, $V_0(t)$ and $V_T(t)$ have been scaled to the same height at $t = 0$.

9.2. Layers

As before we assume monochromatic low intensity excitation falling on the front side of an infinite sheet of dye medium of thickness d , as illustrated in Fig. 9.6. Fluorescence is measured in a detector D at the back. S is the source of emission.

Consider fluorescence within the medium, in a wavelength interval $\lambda + d\lambda$ from a point S acting as source, between cones of half angle θ and $\theta + d\theta$. The pathlength of the light to the back and to the front side of the layer is given by $r_b = x/\cos \theta$ and $r_f = d - x/\cos \theta$, respectively. The fraction of radiation absorbed before reaching the medium boundary is therefore:

$$1 - 10^{-\epsilon(\lambda)c \cdot x/\cos \theta} \tag{9.29}$$

and:

$$1 - 10^{-\epsilon(\lambda)c \cdot (d - x/\cos \theta)}$$

The fraction of radiation emitted by going into the cone slice is:

$$\frac{1}{2} \sin \theta \, d\theta \tag{9.30}$$

Thus, the fraction of radiation absorbed for isotropic emission from S is:

$$\frac{1}{2} \left[\int_0^{\pi/2} (1 - 10^{-\epsilon(\lambda)c \cdot x/\cos \theta}) \sin \theta \, d\theta + \int_0^{\pi/2} (1 - 10^{-\epsilon(\lambda)c \cdot (d - x/\cos \theta)}) \sin \theta \, d\theta \right] \tag{9.31}$$

This equation can be integrated numerically for specific values of $\epsilon(\lambda)c$ and x . Some special cases have been discussed in the literature [21,22].

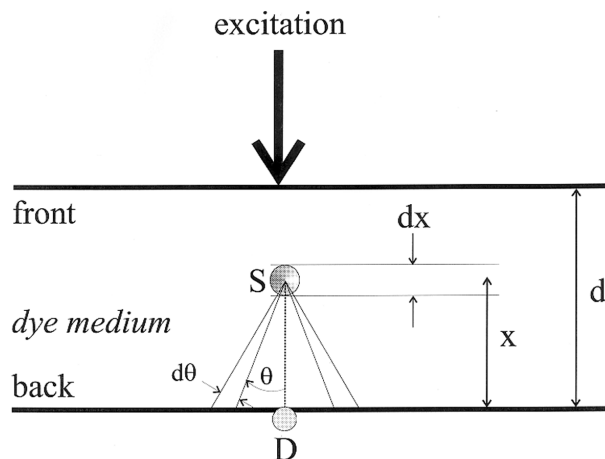


Fig. 9.6. Infinitely extended thin layer.

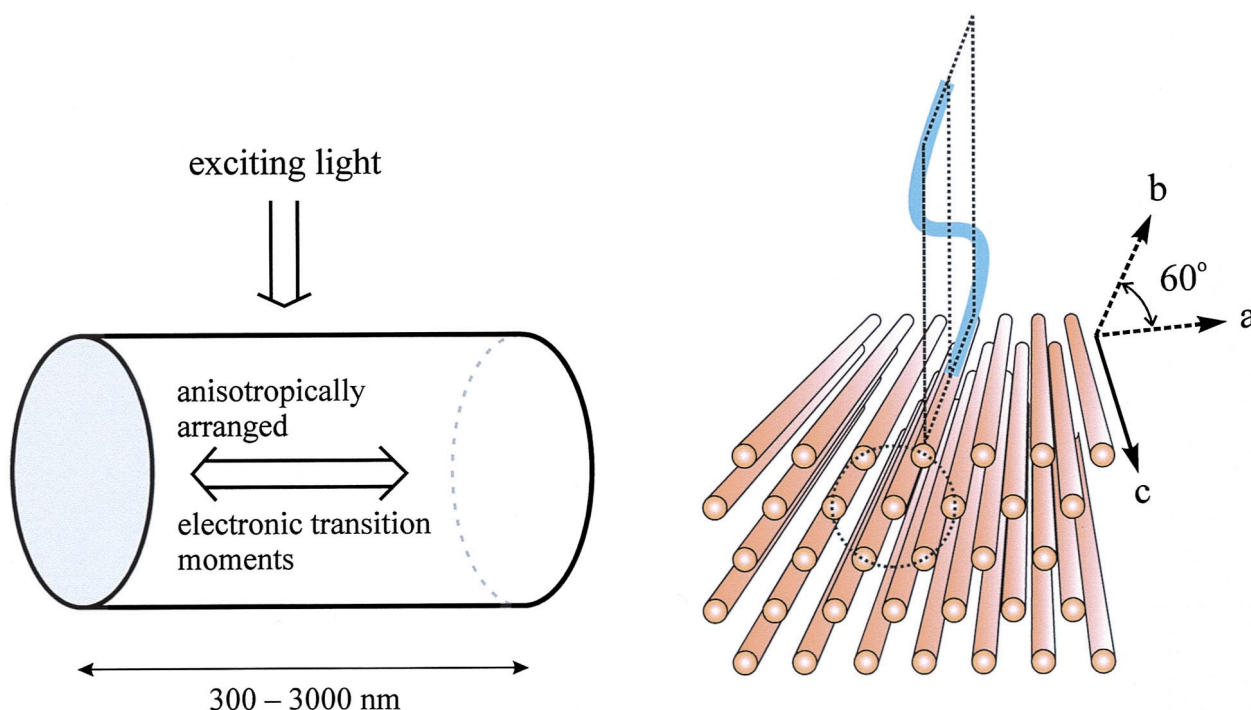


Fig. 9.7. Schematic view of a POPOP-loaded zeolite L nanocrystal. Left: side view of the morphology, size and anisotropy of the material. Right: front view of a few individual channels filled with dye molecules with electronic transition moments aligned along the axis of the channels. The polarization of light which can be absorbed is illustrated.

9.3. Nanocrystals

We now consider a dye-loaded zeolite L nanocrystal in the size regime studied in our group which is in the range 300–3000 nm. In Fig. 9.7 we illustrate the morphology and the pronounced optical anisotropy of a material loaded with POPOP. Some individual channels are illustrated. Only light polarized along the c -axis can be absorbed or emitted because the electronic transition moment of each individual dye molecule is polarized along the c -axis. The wavelength of the light we are working with is in the order of the length of these channels, namely 300–1000 nm. This can cause interesting phenomena which are presently under discussion.

The dye concentration $C(p)$ in mol/L in a zeolite L nanocrystal is related to the occupation probability p as follows:

$$C(p) = \frac{\rho_z}{Mm_z s} p \quad (9.32)$$

ρ_z is the density of the nanocrystal, Mm_z is the

molmass of one unit cell, s is the number of unit cells which form one site and p is the occupation probability. Using $\rho_z = 2.17 \text{ g/cm}^3$, $Mm_z = 2883 \text{ g/mol}$ and $s = 2$, we obtain:

$$C(p) = (0.376 \text{ mol/l})p \quad (9.33)$$

This relation is now used to consider the penetration depth of light falling on such a material. A discus-

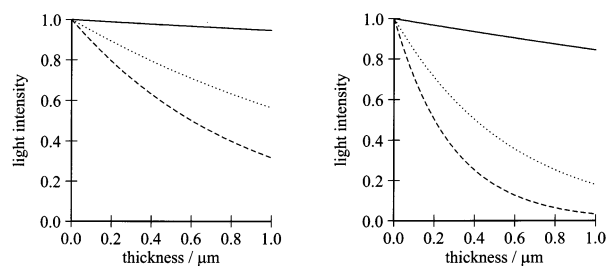


Fig. 9.8. Penetration depth calculated for three different concentrations: 0.005 M (solid), 0.05 M (dotted) and 0.1 M (dashed). An extinction coefficient of $\epsilon = 50\,000 \text{ M}^{-1} \text{ cm}^{-1}$ was used. Left: isotropic orientation. Right: anisotropic orientation.

Table 9.2

Experimental and calculated spectral shifts of the fluorescence spectrum of pyronine zeolite L (700 nm average length) of different loading

p	c/M	λ_{\max}/nm	$\Delta\lambda_{\max}/\text{nm}$			a_{tot}	
			Exp.	Exp.	Calc.		
						Isotropic	Anisotropic
0.005	0.002	515.7	0.0	0.0	0.0	0.004	0.011
0.016	0.006	517.1	1.4	0.0	1.3	0.011	0.033
0.035	0.013	519.7	4.0	0.7	2.7	0.024	0.067
0.070	0.026	522.4	6.7	2.0	4.7	0.046	0.112
0.140	0.052			3.3	6.7	0.087	0.205
0.280	0.104			5.4	9.5	0.153	0.308

sion of diffraction phenomena is postponed and we only discuss the penetration depth of a thin infinite layer. In this case, the light intensity as a function of the thickness can simply be calculated from Eq. (9.1) by drawing $1 - a(\lambda)$ as a function of the thickness r . The results illustrated in Fig. 9.8 show that for organic dyes with their large oscillator strengths penetration depths of less than 500 nm can be realized. This makes such materials very interesting.

We are now prepared to discuss the influence of self-absorption and re-emission on the fluorescence spectrum of these materials. Eq. (9.2) is used to calculate the total fraction of absorbed photons a_{tot} . The spectral shift of the fluorescence spectrum is calculated by means of Eq. (9.3). In Table 9.2 experimental values on thin pyronine zeolite L (700 nm) layers on quartz plates are reported and compared

with the theoretical values. Fig. 9.9 shows the corresponding experimental luminescence spectra. Theoretical values obtained for anisotropic situations are also added for comparison. It is obvious that the anisotropy also influences this aspect of the material. The calculation underestimates the experimentally observed shift, but the general trend is well reproduced. One of the reasons for the larger experimentally observed shift may be that the experiments were done on thin layers, but not on monolayers. This point must be further investigated.

10. Very fast energy migration

We recently reported extremely fast electronic excitation energy migration along the axis of cylindrical crystals of pyronine-loaded zeolite L nanocrystals modified on both ends with oxonine as luminescent traps [10]. The antenna property of this system is governed by Förster-type energy migration. Because of the pronounced anisotropy of the material we expect that the polarization of the donor–donor self-absorption and re-emission is the same as the polarization of the absorbed and of the emitted light as indicated in Fig. 10.1.

Two kinds of stationary experiments give useful information on the energy migration characteristics: one is to measure the trapping efficiency as a function of the loading and the other is to measure it as a function of the length of the nanocrystals. Both have been carried out by us [10]. The trapping efficiency T_{∞} is equal to the sum of the excitation probabilities of all trapping sites at infinite time after irradiation. In a system where donors and traps have

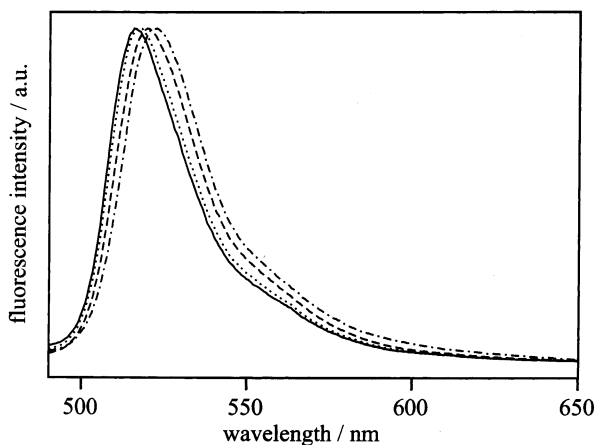


Fig. 9.9. Scaled fluorescence spectra of thin pyronine zeolite L layers at different loading: $p = 0.005$ (solid), $p = 0.016$ (dotted), $p = 0.035$ (dashed), $p = 0.070$ (dashdot).

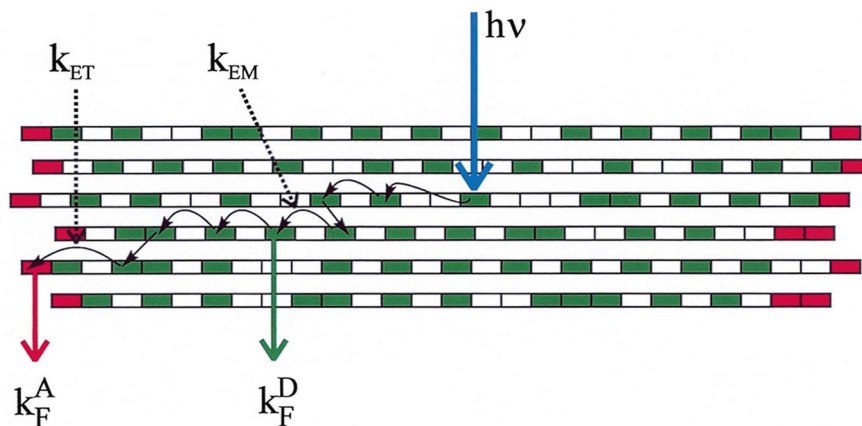


Fig. 10.1. Main processes occurring in the energy migration from an excited donor (pyronine) taking place mainly along the cylinder axis because of geometrical constraints. The excitation energy is finally trapped by an acceptor (oxonine) located at the end of the zeolite L nanocrystal which emits red light. k_{ET} is the rate constant for energy transfer, while k_F^A and k_F^D are the rate constants for fluorescence of the acceptor (red rectangles) and the donor (green rectangles), respectively. Polarization of the absorbed and of the emitted light is indicated.

a luminescence quantum yield of one and where the traps are excited exclusively by receiving energy from the donors, the trapping efficiency corresponds to the ratio of the luminescence intensity of the traps divided by the total luminescence. In the experiments described here, the donors which absorb light are pyronine while the traps are oxonine molecules, both of which have a quantum yield of nearly 1. Their luminescence intensity is given by I_{py} and I_{ox} , respectively. We have shown that for this system the following simple relation holds [6,10].

$$T_\infty = \frac{I_{ox}}{I_{py} + I_{ox}} \quad (10.1)$$

An experiment which demonstrates the extremely fast energy migration is illustrated in Fig. 10.2. The experiments were carried out with zeolite L nanocrystals of 700 nm average length. The samples were suspended in water. Effective energy migration lengths of up to 166 nm were observed (see table 1 of Ref. [10]). Note that only the emission maximum of the donor (pyronine) shifts to longer wavelength with increasing loading. The emission maximum of the acceptor which is oxonine, placed at both ends of the cylindrical crystals, does not shift. The reason for this is that its concentration is always low and the same in each experiment.

We have recently improved the material and the experimental techniques. Glass plates were coated

with a thin dye-loaded zeolite L layer. The effective energy migration length [6] estimated from the results is in the order of 200 nm [24].

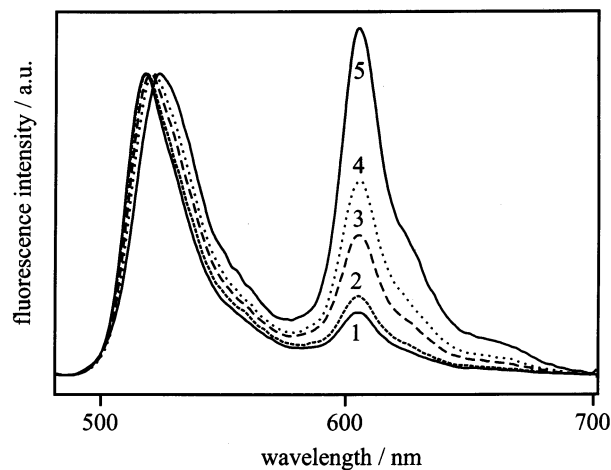


Fig. 10.2. Energy migration in pyronine zeolite L nanocrystals as observed by the oxonine fluorescence at different pyronine loadings p_{py} , increasing from 1 to 2, 3, 4, 5: 1, $p = 0.03$; 2, $p = 0.06$; 3, $p = 0.12$; 4, $p = 0.24$; 5, $p = 0.48$. The material was suspended in water. We show the relative intensity of fluorescence spectra recorded after specific excitation of only pyronine molecules at 470 nm scaled to the same height at the maximum of the pyronine emission. The amount of front-back located oxonine traps corresponds on average to one molecule at the front and one at the back of each channel in all samples [9].

11. External trapping

So far experiments on energy transfer, energy migration and trapping taking place inside the dye-loaded zeolite L nanocrystals have been discussed. We now discuss radiationless energy transfer to an external acceptor. The principle of an experiment to probe for energy transfer to a trap located at the outside of a nanocrystal is illustrated in Fig. 11.1. Energy is absorbed by a donor located somewhere inside the crystal, it then migrates very quickly to one of the ends of the cylinder where it is trapped by an acceptor. The latter is able to transfer the energy to an external acceptor. The internal acceptor is not necessary, but it is convenient in many cases.

We have carried out a number of such experiments from which we report two, both realized without an internal acceptor. The first consists of adsorbing a molecule which is too large to enter the channels of zeolite L. It should have a large spectral overlap with the donor molecules located inside the crystals. Cationic dyes such as methyleneblue, ethyleneblue, cresylechtviolet and others readily adsorb at the zeolite L crystal surface and they do not enter the channels. In Fig. 11.2 we show a result obtained with cresylechtviolet. It illustrates that external trapping works well. Experiments with methyleneblue as an external trap lead to similar results.

The second experiment was carried out on a thin oxonine-loaded zeolite L layer on glass onto which in one case different amounts of gold (Fig. 11.3) and in the other case different amounts of silicon were evaporated. In both cases quenching of the oxonine luminescence was observed. It was more pronounced for gold than for silicon. Care was taken that light absorption by the material deposited on the nanocrystal did not disturb the experiment.

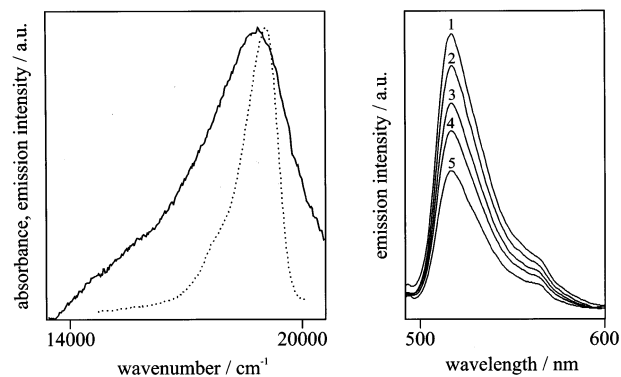


Fig. 11.2. Left: spectral overlap between the absorption spectrum of the external quencher (cresylechtviolet, solid) and the fluorescence spectrum of the internal donor (pyronine, dotted). Right: fluorescence of pyronine as a function of the amount of cresylechtviolet adsorbed on the outside of the nanocrystals. The pyronine loading was about 0.006. The amount of cresylechtviolet on the outside increases from spectra 1–5. Its concentration was in each case so low, that possible absorption of the pyronine luminescence by the quencher remained unimportant.

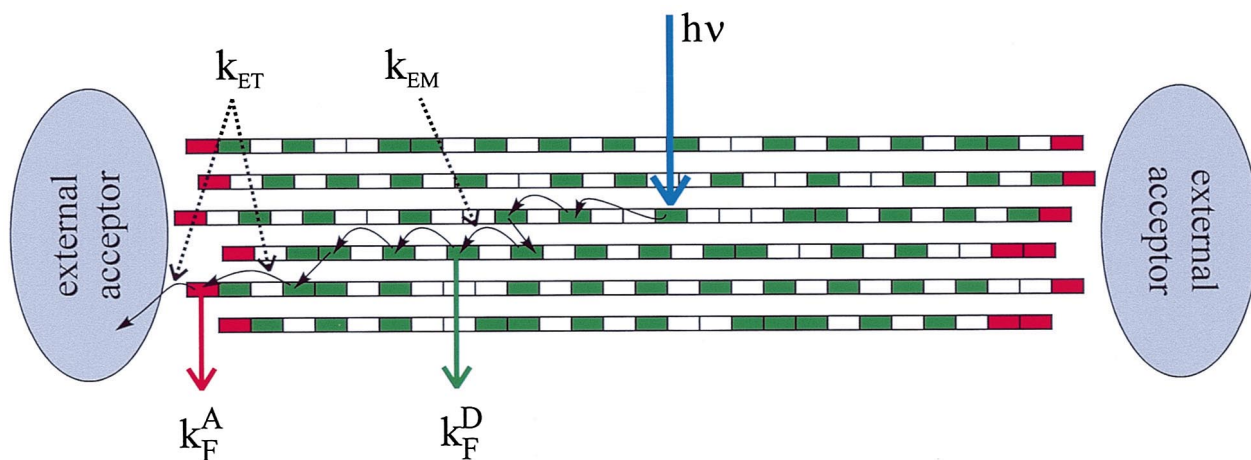


Fig. 11.1. External trapping of energy absorbed somewhere by a donor inside of a dye-loaded zeolite L nanocrystal. Energy migration takes place mainly along the cylinder axis because of geometrical constraints. The excitation is trapped by an acceptor located at both ends. The thus excited acceptor either transfers its energy to an external acceptor or relaxes by emitting a photon, depending on the conditions.

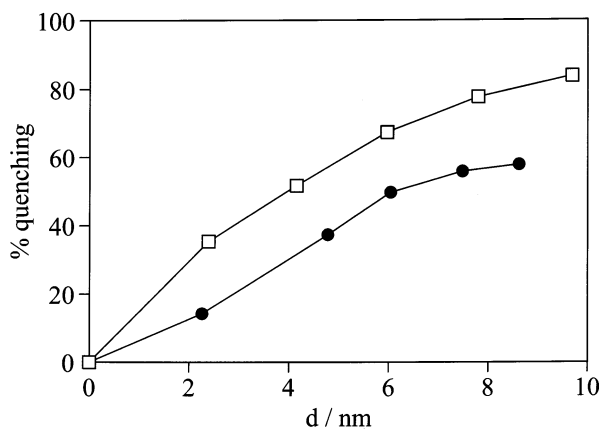


Fig. 11.3. Quenching of the oxonine luminescence of oxonine-loaded zeolite L nanocrystals (coated as a thin layer on glass) by vapor-deposited gold. The oxonine loading was about 0.065 (empty squares) and 0.025 (circles). The absolute thickness d of the gold layer given in Å could not be measured precisely in these experiments, but the estimated values are sufficiently precise.

12. Conclusions

We conclude that the fascinating properties of the systems discussed in this article give rise to much speculation on applications. The antenna properties can perhaps be used in realizing a new type of photovoltaic device in which the absorption of light and the creation of an electron-hole pair are spatially separated. Contributions to new imaging techniques, data storage, specific biological and medical applications can be imagined. The antenna nanocrystals can also be regarded as candidates for realizing a new type of electronic screen with high spatial resolution. The pronounced anisotropy, the geometrical constraints, the high concentration of monomers which can be realized and the extremely fast energy migration have great potential to lead to new photophysical phenomena.

Acknowledgements

This work was supported by the Swiss National Science Foundation Project NFP 36(4036-043853), project NF 2000-053414/98/1 and by the Bundesamt für Energie, Project 10441. We thank Dr Niklaus

Gfeller for many interesting discussions and suggestions. We also thank René Bühler for preparing the pyronine and for carrying out the experiments reported in Figs. 5.1 and 6.2.

References

- [1] This work was presented as a plenary lecture at the VIIth European Conference On Solid State Chemistry (Sept. 15-18, 1999, Madrid) by G. Calzaferri.
- [2] G. Calzaferri, *Chimia* 52 (1998) 525 and references therein.
- [3] G. Calzaferri, in: M. Anpo (Ed.), *Photofunctionalized Zeolites*, Nova Science, 2000 in press.
- [4] D.W. Breck, *Zeolite Molecular Sieves*, Wiley, New York, 1974.
- [5] W.M. Meier, D.H. Olson, Ch. Baerlocher, *Atlas of Zeolite Structure Types*, Elsevier, London, 1996.
- [6] N. Gfeller, G. Calzaferri, *J. Phys. Chem. B* 101 (1997) 1396.
- [7] E.G. McRae, M. Kasha, *Phys. Prog. Rad. Biol.*, Academic Press, New York, 1964, p. 23.
- [8] (a) Th. Förster, *Ann. Phys. (Leipzig)* 2 (1948) 55. (b) Th. Förster, *Fluoreszenz organischer Verbindungen*, Vandenhoeck & Ruprecht, Göttingen, 1951.
- [9] N. Gfeller, S. Megelski, G. Calzaferri, *J. Phys. Chem. B* 102 (1998) 2433.
- [10] N. Gfeller, S. Megelski, G. Calzaferri, *J. Phys. Chem. B* 103 (1999) 1250.
- [11] P. Lainé, R. Seifert, R. Giovanoli, G. Calzaferri, *New J. Chem.* 21 (1997) 453.
- [12] M. Pauchard, A. Devaux, G. Calzaferri, *Chem. Eur. J.*, in press.
- [13] B. Hennessy, S. Megelski, C. Marcolli, V. Shklover, Ch. Baerlocher, G. Calzaferri, *J. Phys. Chem. B* 103 (1999) 3340.
- [14] T. Ohsuna, Y. Horikawa, K. Hiraga, *Chem. Mater.* 10 (1998) 688.
- [15] A. Kunzmann, R. Seifert, G. Calzaferri, *J. Phys. Chem. B* 103 (1999) 18.
- [16] G. Calzaferri, N. Gfeller, *J. Phys. Chem.* 96 (1992) 3428.
- [17] (a) F. Binder, G. Calzaferri, N. Gfeller, *Sol. Ener. Mat. Sol. Cells* 38 (1995) 175. (b) F. Binder, G. Calzaferri, N. Gfeller, *Proc. Ind. Acad. Sci. (Chem. Sci.)* 107 (1995) 753.
- [18] M. Klessinger, J. Michl, *Lichtabsorption und Solvatochromie organischer Moleküle*, VCH, Weinheim, 1989, p. 123.
- [19] D. Brühwiler, N. Gfeller, G. Calzaferri, *J. Phys. Chem. B* 102 (1998) 2923.
- [20] G. Calzaferri, R. Rytz, *J. Phys. Chem.* 99 (1995) 12141.
- [21] P.R. Hammond, *J. Chem. Phys.* 70 (1979) 3884.
- [22] J.S. Batchelder, A.H. Zewail, T. Cole, *Appl. Optics* 18 (1979) 3090.
- [23] J. Baumann, G. Calzaferri, T. Hugentobler, *Chem. Phys. Lett.* 116 (1985) 66.
- [24] S. Megelski, PhD thesis, University of Bern, June, 2000.